Formation of a rain shadow: O and H stable isotope records in authigenic clays from the Siwalik Group in eastern Bhutan

Djordje Grujic[a], Gwladys Govin[b], Laurie Barrier[c], Bodo Bookhagen[d], Isabelle Coutand[a], Beth Cowan[a], Michael T. Hren[e], Yani Najman[b]

[a]Department of Earth Sciences, Dalhousie University, PO BOX 15000 Halifax, NS, B3H 4R2, Canada. dgrujic@dal.ca

[b]Lancaster Environment Centre, Lancaster University, Lancaster, LA1 4YQ, UK

[c]Institut de Physique du Globe de Paris, Sorbonne Paris Cité, Université Paris Diderot, UMR7154 CNRS, F-75005 Paris, France

[d]Institute of Earth and Environmental Science, University of Potsdam, 14476 Potsdam-Golm, Germany

[e]Department of Chemistry, University of Connecticut, Storrs, Connecticut 06269, USA

Key Points

1. Isotopic composition of authigenic clays in sediments of the Himalayan foreland basin indicates environmental changes since Late Miocene.
2. Surface uplift of the Shillong Plateau led to the formation of a rain shadow in its lee, in the Himalayan foreland.
3. The mean annual precipitation over the foreland basin of the eastern Bhutan Himalayas has decreased by a factor of 1.7-2.5.

Abstract

We measure the oxygen and hydrogen stable isotope composition of authigenic clays from Himalayan foreland sediments (Siwalik Group), and from present day small stream waters in eastern Bhutan to explore the impact of uplift of the Shillong Plateau on rain shadow formation over the Himalayan foothills. Stable isotope data from authigenic clay minerals (<2 μm) suggests the presence of three palaeoclimatic periods during deposition of the Siwalik Group, between ~7 and ~1 Ma. The mean $\delta^{18}O$ value in palaeo-meteoric waters, which were in equilibrium with clay minerals, is ~2.5‰ lower than in modern meteoric and stream waters at the elevation of the foreland basin. We discuss the factors that could have changed the isotopic composition of water over time and we conclude that: (a) The most likely and significant cause for the increase in meteoric water $\delta^{18}O$ values over time is the "amount effect", specifically, a decrease in mean annual precipitation. (b) The change in mean annual precipitation over the foreland basin and foothills of the Himalaya is the result of orographic effect caused by the Shillong Plateau's uplift. The critical elevation of the Shillong Plateau required to induce significant orographic precipitation was attained after ~1.2 Ma. (c) By applying scale analysis, we estimate that the mean annual precipitation over the foreland basin of the eastern Bhutan Himalayas has decreased by a factor of 1.7-2.5 over the last one to three million years.

Keywords

Authigenic clay, stable isotope, orographic precipitation, Siwaliks, Himalaya, foreland basin

1. Introduction

Case studies on interactions between tectonics, climate, and erosion traditionally compare the pattern of erosion rates or the timing of activation of major tectonic structures with the spatial distribution of modern precipitation. However, these studies commonly lack either evidence that current climatic conditions operated during the time range for which erosion rates are usually estimated or a quantitative assessment on past climate change. Furthermore, for the case of active critical Coulomb wedges, it has been analytically demonstrated (e.g., [*Whipple*, 2009] that climate change must be recent (1-2 Ma) for its effect on landscape or structures to be preserved.

It is equally difficult to isolate the respective contributions of tectonics and climate on erosion rates [*Champagnac et al.*, 2012; *Von Blanckenburg*, 2005; *Whipple*, 2009]. Whereas on the global scale there is strong, yet disputed, evidence for higher erosion rates in mountain ranges due to Quaternary glaciation (e.g., [*Herman et al.*, 2013; *Willenbring and von Blanckenburg*, 2010], a direct connection between climate and erosion is less evident at the regional scale in active orogens.

Therefore, to demonstrate through observational studies that climate change has a measurable impact on upper crustal exhumation/erosion in an active orogen, we need to identify a region that, in the geological past, has undergone sufficiently large changes in precipitation amount for climate-modulated erosion to outpace tectonically-driven rock uplift and exhumation. One such region is the Himalayan orogenic front and its foreland basin in eastern Bhutan. It is the only segment of the Himalayan foreland with an elevated, tectonically active terrane: the Shillong Plateau. During the Indian Summer Monsoon (ISM), warm moisture-bearing air masses moving northwards, from the Bay of Bengal toward the Himalayan range, meet the Shillong Plateau, rise, cool and are condensed along the southern flank of the plateau (Fig. 1), making it one of the wettest area on Earth. It has been suggested, but not demonstrated, that this orographic precipitation has significantly reduced leeward precipitation along the foothills of the Himalaya [*Bookhagen and Burbank*, 2010; *Grujic et al.*, 2006]. It has been also observed that the segment of the Himalaya in the lee of the Shillong plateau, compared to the segments to the east and west, undergoes slower erosion rates since the Pliocene [*Coutand et al*., 2014], and has different seismotectonic characteristics [*Marechal et al*., 2016; *Singer et al*., 2017]. Topographic rise of the plateau occurred during the Pliocene [*Biswas et al.*, 2007; *Najman et al.*, 2016; *Rosenkranz et al*., 2018; *Govin et al*., 2018], which was long after the ISM was established (Section 2.1). We can, therefore, ask following questions: When did the plateau reach the threshold elevation to cause orographic precipitation on its southern flank? Did leeward precipitation simultaneously decrease? Can we quantify this change in space and time?

The research objective of this study is to discern whether the Siwalik sediments can provide evidence for the surface uplift of the Shillong Plateau and its impact on the precipitation pattern of the eastern Himalayas, by characterising the climate trends during Siwalik deposition over the last 7 Ma using stable isotope proxies. We emphasise that our study represents a step toward understanding the interactions between climate and tectonics and focuses more on the potential causes of regional climate change (formation of an orographic rain shadow) rather than an interpretation of all climate-tectonic interactions (e.g. quantifying the change in erosion rate with precipitation).

2. Background

2.1 The Indian summer monsoon

Climate simulations and palaeoclimate data (e.g., [*Licht et al.*, 2014; *Roe et al.*, 2016] conclude that Asian monsoon-like conditions were present at least as far back as 40 Ma. On a million-year timescale, there are two conspicuous periods of geologically recent climate change in Asia. Palaeoclimate data suggest that a range of climatic changes occurred around 10 Ma throughout the regions surrounding Tibet [*Dettman et al.*, 2001; *Hoorn et al.*, 2000; *Quade et al.*, 1989; *Quade et al.*, 1995]. These changes apparently marked a strengthening of the South Asian monsoon. Secondly, nearly all palaeoclimate proxies on Earth show a change between ~4 and 2.5 Ma, when northern hemisphere cooling accelerated. Pollen, foraminifera, and $\delta^{13}C$ analyses from north-west India, the northern Indian Ocean, and the Arabian Sea indicate a marked dry, semi-arid climatic regime and a weaker monsoon in the Himalayas [*Thomas et al.*, 2002], consistent with the global Pleistocene cooling that started at 2.7 Ma.

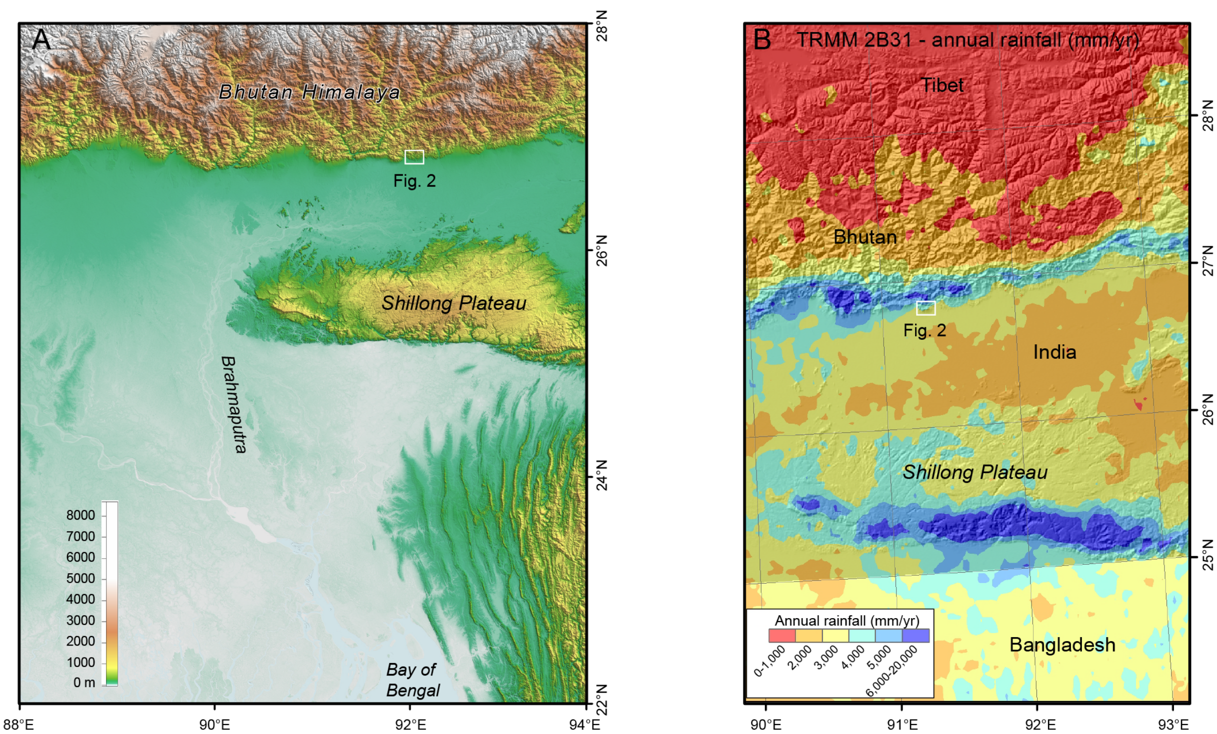

Figure 1. Landscape (a) and Indian summer monsoon precipitation (b) in the eastern Himalayas, Shillong Plateau, and the foreland. (a) Digital elevation map generated with GeoMapApp (http://www.geomapapp.org.) using the, the Global Multi-Resolution Topography Synthesis

basemap [*Ryan et al.*, 2009]. (b) Mean annual rainfall is from the Tropical Rainfall Measuring Mission (TRMM) calibrated 12-year average product 2B31 [*Bookhagen and Burbank*, 2010].

On a regional scale, based on the difference in distribution of ISM precipitation across eastern and western Bhutan, [*Grujic et al.*, 2006] hypothesised that uplift of the Shillong Plateau at the Miocene-Pliocene boundary decreased precipitation in eastern Bhutan. The decrease in precipitation over the foothills might have been sufficient to generate a transient landscape characterised by the presence of palaeolandscape remnants [*Grujic et al.*, 2006] and to alter the geometry of the foreland fold-and-thrust belt [*Hirschmiller et al.*, 2014]. Alternatively, the transient landscapes may have been formed by tectonic processes [*Adams et al.*, 2016].

At present, the Shillong Plateau receives approximately 11000 mm/yr of rainfall on its southern slope [*Breitenbach et al.*, 2010], creating a rain shadow on its leeward side (Fig. 1) where mean annual precipitation rate decreases to ~3500 mm/yr at Samdrup Jongkhar in eastern Bhutan (Royal Government of Bhutan, 2017).

2.2 The Shillong Plateau

The Shillong Plateau, within the Himalayan foreland, is a 1600 m-high orographic barrier to prevailing winds transporting moist air from the Bay of Bengal northwards to the Himalayan front (Fig. 1). It has been suggested that surface uplift of the plateau reduced the mean annual precipitation in the downwind direction along the Himalayan front of eastern Bhutan [*Biswas et al.*, 2007; *Bookhagen and Burbank*, 2010; *Grujic et al.*, 2006]. Initial basement rock uplift, starting at least 15-9 Ma ago, did not generate significant surface uplift until the basement became exposed at the Miocene-Pliocene transition, decreasing erosion rates and resulting in plateau surface uplift after ~4-3 Ma [*Biswas et al.*, 2007], 3.5-2 Ma [*Najman et al.*, 2016], around 4.5 Ma [*Rosenkranz et al*., 2018] or at ca. 5.2–4.9 Ma [*Govin et al*. 2018]. Our hypothesis is that once the Shillong Plateau reached a sufficient elevation to cause orographic precipitation on its southern side by stable upslope ascent of warm moisture-bearing air masses ([*Roe*, 2004], and references therein), this decreased the amount of precipitation on the leeward side of the plateau, in the foothills of the eastern Bhutanese Himalayas to the north. This regional climatic change—in addition to the signal caused by the assumed synoptic changes of the ISM—should be evidenced by a shift in the stable isotope composition of the coevally deposited foreland sediments.

2.3 The Siwalik Group

The Dungsam Chu section, located in the foothills of the Himalayas in eastern Bhutan (Fig. 2), is composed of synorogenic Neogene-Pleistocene foreland sediments of the Siwalik Group forming a ~2200 m-thick section with a continuous exposure on freshly eroded stream banks.

The section belongs to the modern Himalayan foreland fold-and thrust belt, as defined by [*Hirschmiller et al.*, 2014]. It is bounded to the north by the Main Boundary Thrust (MBT), along which the Lesser Himalayan Sequence (LHS) has been thrust over the Siwalik Group, and to the south by the Main Frontal Thrust (MFT), which juxtaposes the Siwalik Group strata against the modern Brahmaputra plain alluvial sediments (Fig. 2). All three lithostratigraphic subgroups, the Lower, Middle, and Upper Siwaliks (for definitions, see *Quade et al.* [1995]) are exposed along the Dungsam Chu section.

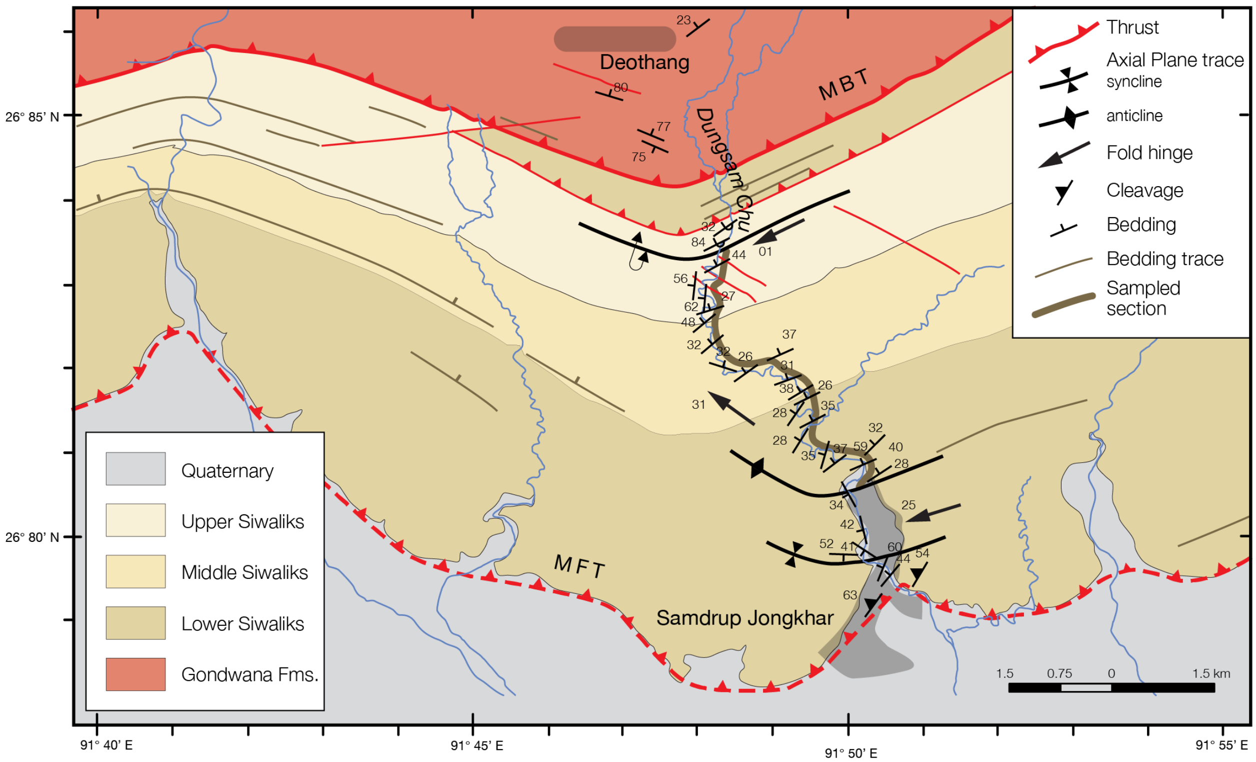

Figure 2. Geological map of the eastern Bhutan Sub-Himalayas. MBT: Main Boundary Thrust, MFT: Main Frontal Thrust. The studied section of the Siwaliks along Dungsam Chu is indicated by a thick brown line.

In an accompanying study, we established the detailed stratigraphy and sedimentology along the Dungsam Chu section in the eastern Bhutan Himalaya [*Coutand et al.*, 2016]. We revised the exclusively lithological subdivision of the Siwaliks by identifying 12 facies and four facies associations representative of distinct depositional palaeoenvironments. Furthermore, we dated Siwalik deposition along the Dungsam Chu section, using magnetostratigraphy constrained by vitrinite reflectance data combined with detrital apatite fission-track dating (Fig. 3, [*Coutand et al.*, 2016], to the latest Miocene and the Pleistocene, between ~7.2 Ma and ~1 Ma. Unit 1 deposits are interpreted as different parts of a river-dominated deltaic system, developed in either a lacustrine or marine environment between < 7.2 Ma and 6.4 Ma. Unit 2 deposits (6.4 - 5 Ma) represent a river- and storm-dominated deltaic depositional environment, which transitioned after 5 Ma into Unit 3 deposits, a sandy alluvial environment. Over a sharp transition Unit 3 shifts to Unit 4 (~3.8 and > 1.2 Ma), representing a gravelly alluvial environment. Of the traditional Siwalik subgroups, the Lower to Middle Siwalik boundary is dated at ~6 Ma, and the Middle to Upper Siwalik boundary at ~3.8 Ma. The youngest dated beds at the top of the section are ~1.2 Ma old [*Coutand et al.*, 2016]. Paleosols were identified throughout the section [*Coutand et al.*, 2016] and samples for this study were collected from each pedogenically modified horizon.

Figure 3. Siwalik stratigraphy along the Dungsam Chu section. (a) Stratigraphic column and environmental units (as defined by *Coutand et al.* [2016]. Unit 1: river-dominated deltaic system, Unit 2: river- and storm-dominated system, Unit 3: sandy alluvial system, Unit 4: gravelly alluvial system. (b) Palaeosol sample locations. Samples were collected from each pedogenically modified horizon recognised in the field. Each of them is at a paleosol level recognised in the field. (c) Polarity zones defined for the section and the proposed correlations to (d) the geomagnetic polarity time scale of *Gradstein and Ogg* [2012]. (a), (c) and (d) after *Coutand et al.* [2016].

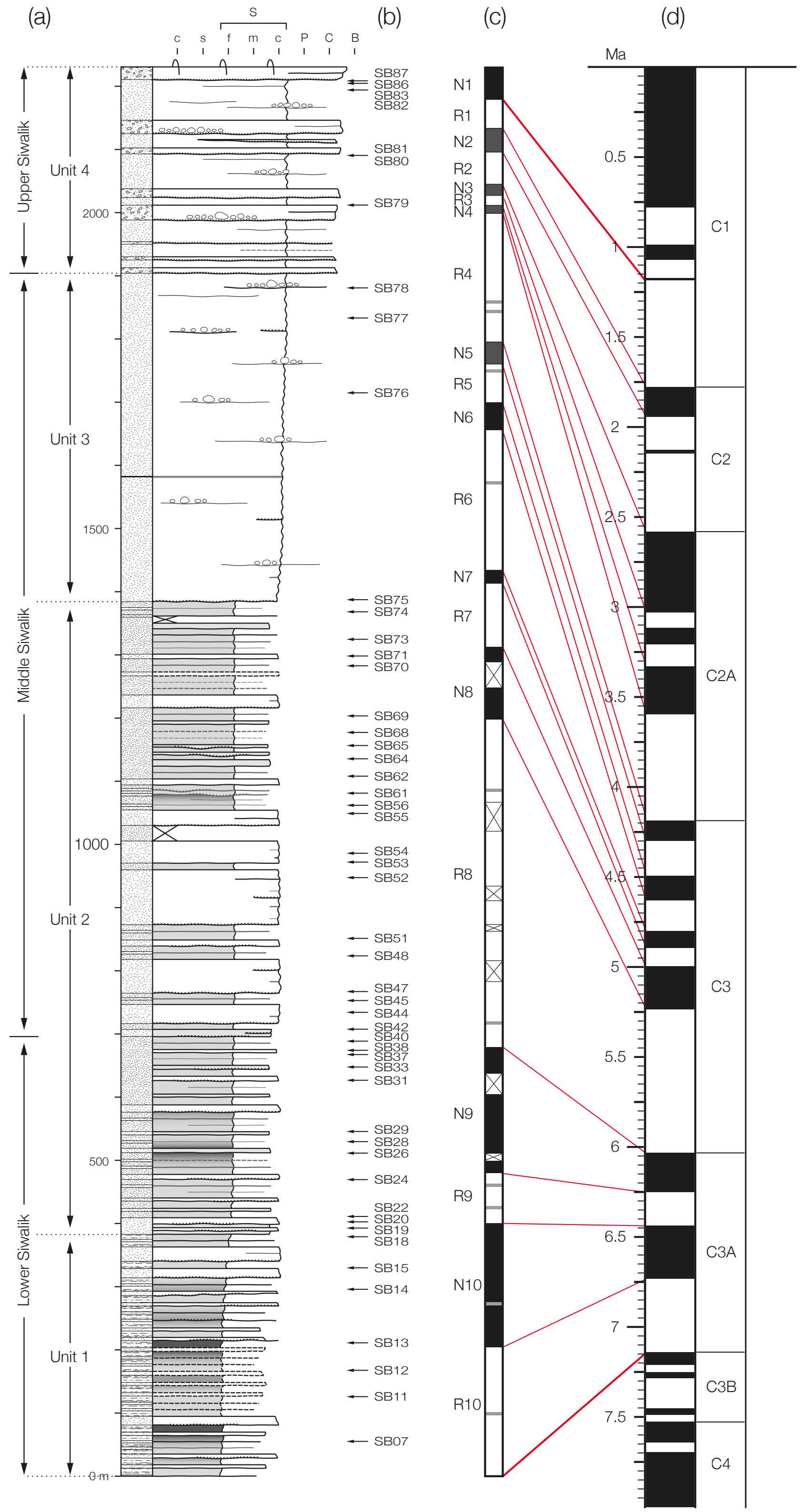
(a)
(b)
(c)
(d)
S
c s f m c P C B
Upper Siwalik
Middle Siwalik
Lower Siwalik
Unit 4
Unit 3
Unit 2
Unit 1
2000
1500
1000
500
0 m
SB87
SB86
SB83
SB82
SB81
SB80
SB79
SB78
SB77
SB76
SB75
SB74
SB73
SB71
SB70
SB69
SB68
SB65
SB64
SB62
SB61
SB56
SB55
SB54
SB53
SB52
SB51
SB48
SB47
SB45
SB44
SB42
SB40
SB38
SB37
SB33
SB31
SB29
SB28
SB26
SB24
SB22
SB20
SB19
SB18
SB15
SB14
SB13
SB12
SB11
SB07
N1
R1
N2
R2
N3
R3
N4
R4
N5
R5
N6
R6
N7
R7
N8
R8
N9
R9
N10
R10
Ma
0.5
1
1.5
2
2.5
3
3.5
4
4.5
5
5.5
6
6.5
7
7.5
C1
C2
C2A
C3
C3A
C3B
C4

3. Materials and Methods

3.1. Samples

3.1.1 Meteoric water

There are no long-term measurements of isotopic composition of rain or meteoric water in the wider region of the study area. Isotopic composition of rivers in the foothills and the foreland of the Himalaya [*Bhattacharya et al.*, 1985; *Ramesh and Sarin,* 1992; *Rozanski et al*., 2001; *Lambs et al*., 2005; Gajurel et al., 2006 (and references therein), *Achyuthan et al*., 2013] could potentially constrain the values of stable isotopes in the foreland basin of the Bhutan Himalaya. However, the published isotopic data cover the range along the meteoric water line from $\delta^{18}O$ =-3 to -12‰, and the sampling has not been systematic to distinguish the seasonal from latitudinal variations. All these short-term measurements are also biased because the ISM values are depleted relative to dry season values [e.g., *Breitenbach et al*., 2010]. Consequently, we decided to empirically derive the present day isotopic composition of water at the foreland basin elevation (50-150 m) based on isotopic composition versus elevation. Stream water samples were collected along a north-south transect across the study area at elevations from 206 m to 3608 m (Figs. 6 a & b, Table S1). Although there is uncertainty in the spatial and temporal distribution of precipitation represented in river water, its tendency to integrate precipitation makes it a better representation of monthly or annual weighted averages than individual precipitation events [*Kendall and Coplen*, 2001]. The isotopic composition of the modern surface water was derived from a set of local small stream-water samples collected during a couple of days in October 2007, May 2008, and November 2010 along a 60 km-long, NS-trending transect, at elevations between 206 and 3608 m (Table S1).

3.1.2 Pedogenic clays

Pedogenic carbonate concretion deposits in palaeosols have commonly been used to reconstruct palaeoclimatic conditions [*Tabor and Myers*, 2015], however, they are only found, formed, and preserved in moderate- to low-rainfall regions [*Tabor and Myers*, 2015]. Trend towards fewer carbonate concretions in the Siwalik sediments observed from western to eastern sections in Nepal [*Quade et al.*, 1995], and the lack of carbonate nodules in Siwalik sediments of eastern Himalaya (this study and [*Vögeli et al.*, 2017]), suggest that the lateral environmental and climatic differences in the modern Himalaya are representative of long-term climatic patterns [*Vögeli et al.*, 2017]. Nevertheless, in palaeosols lacking soil carbonate, the oxygen and hydrogen isotopic composition of pedogenic clay minerals can be used as an alternative palaeoclimate indicator [*Stern et al.*, 1997]. To achieve the objectives of this study, 87 palaeosol samples were collected along the Dungsam Chu transect in southeastern Bhutan (Fig. 3).

Overall, the palaeosols found within the Siwalik Group are bioturbated, and in the central and western Himalaya, typically enriched in illuvial clays [*DeCelles et al.*, 1998; *Quade et al.*, 1995]. Palaeosols along the Dungsam Chu consist of mudstone, siltstone to sandy siltstone characterised by spheroidal weathering, partial to complete obliteration of original depositional features, root traces, bioturbation, and a lack of carbonate nodules (Fig. 4). Root structures, when present, are typically poorly defined root halos. The upper horizons also exhibit sand or mud-filled clastic dikes. Most of the paleosols have weak grey to red matrix colours with fine to coarse mottling.

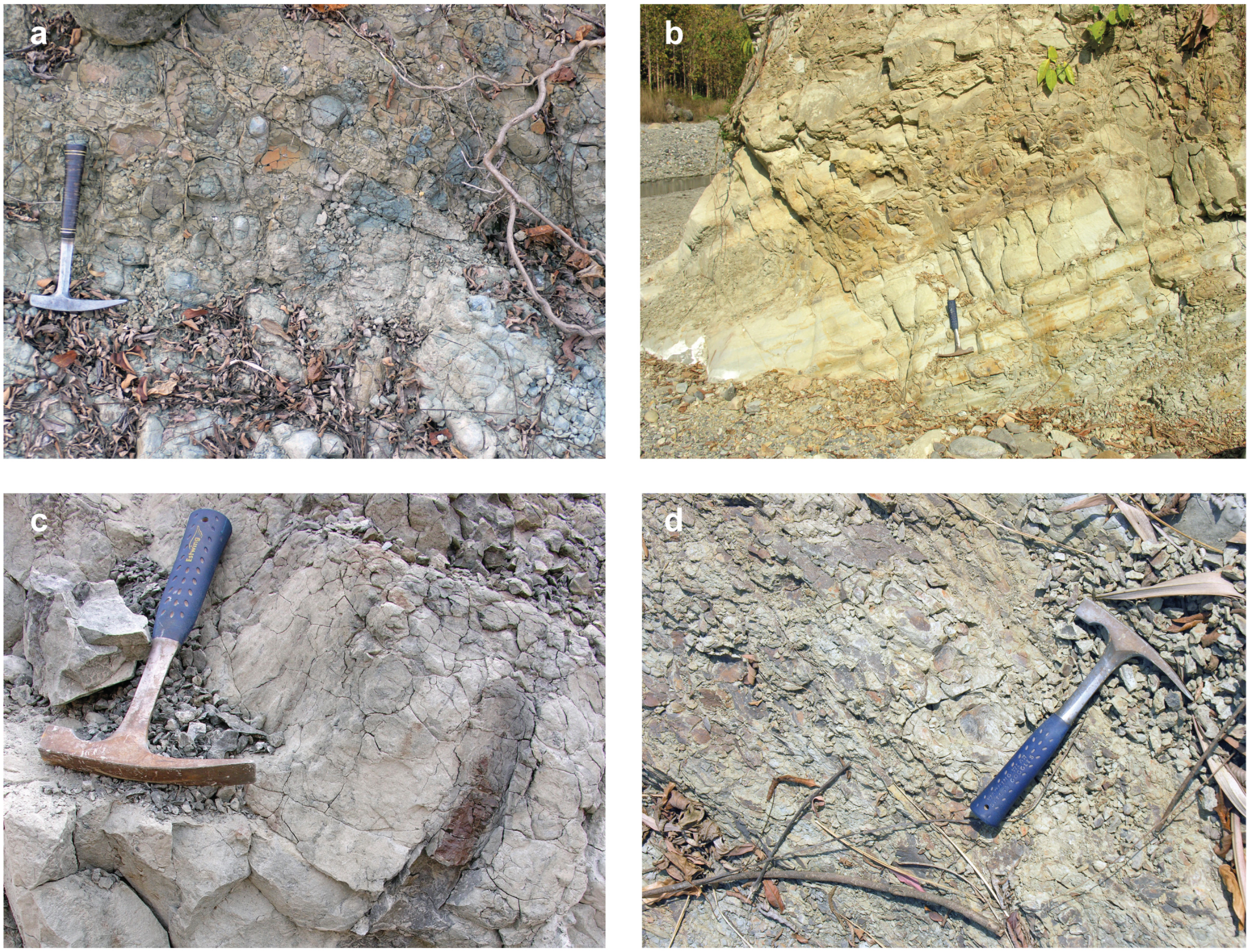

Figure 4. Palaeosol field photographs of a) Spheroidal weathering pattern in varicoloured siltstone. Note the absence of bedding. Unit 1, sample 12 location; b) Unit 2 Sample 30 location; c) Root traces in siltstone. Unit 2, sample 34 location; d) Weathering pattern in siltstone. Unit 2, sample 66 location.

3.2. Clay mineral separation

For the separation of clay minerals, care was taken to avoid diminution of the minerals. Each palaeosol sample was crushed using a mortar and pestle, then broken up using an ultrasonic bath. The sample was then treated with glacial acetic acid (0.3 M) to remove carbonates and 30%

H_2O_2 solution to remove organic matter. After each treatment, the samples were rinsed with deionised water by centrifugation five or six times. After 100 seconds of centrifugation at 800 rpm, and applying Stokes' Law to the machine parameters [*Moore and Reynolds*, 1997], the material left in suspension was the <2 μm size fraction. In hopes of getting a mostly pedogenic clay fraction with further centrifugation of several samples, we isolated grain size fractions <0.4 μm and <0.1 μm. The fractions were suctioned out of the vial and dried in an oven at 60 °C.

3.3. X-ray diffraction (XRD)

Samples for XRD measurements were prepared using the smear method [*Moore and Reynolds*, 1997] by pipetting the suspensions (~5 mg/cm^3) onto glass slides. The X-ray diffractograms were made using an untreated, heated to 500 °C for 2 h, and a glycolated sample (Figure S1) on a Phillips PW 3710 diffractometer (Dalhousie University, Halifax). Details of analytical procedures are described in the Supporting Information S1.1.

3.4. Oxygen and Hydrogen mass spectrometry

The oxygen and hydrogen isotopic compositions of clay minerals were measured by a Finnigan MAT 253 isotope ratio mass spectrometer and a TC/EA coupled to a gas chromatographic column and a mass spectrometer [*Bauer and Vennemann*, 2014], respectively, in the Stable Isotope Laboratory at the University of Lausanne (Switzerland). Oxygen mass spectrometry followed a method outlined in [*Vennemann et al.*, 2001] and the hydrogen mass spectrometry followed the method by [*Bauer and Vennemann*, 2014]. Details of analytical procedures are given in Supporting Information S1.3.

4. Results

4.1 Clay composition

XRD analyses indicate that samples are predominantly composed of clay minerals and fine-grained quartz, and do not contain detrital micas (Table S2). Illite is present in all samples, and kaolin group clays are in all but four samples from the Lower Siwalik subgroup. Smectite is found in about half of the samples throughout the sedimentary section. Chlorite occurs only in samples from Lower Siwalik sediments (Table S2). Furthermore, glauconite is found in samples from the bottom 170 m of the section. These mineral identifications were confirmed with the scanning electron microscopy and energy dispersive spectroscopy (SEM/EDS), and transmission electron microscopy (TEM).

4.2 Clay oxygen and hydrogen isotopes

In samples that have three grain-size fractions (0.1 μm, 0.4 μm, and 2 μm), the $\delta^{18}O$ and δD isotopic data show no consistent relation between grain size and isotopic composition (Table S3). The measured $\delta^{18}O$ and δD Vienna Standard Mean Ocean Water (VSMOW) values of palaeosol clays range from 11.5 to 14.3‰ and from -103.8 to -81.5 ‰, respectively (Fig. 5 and Table S2). Quartz will contain only negligible water therefore an isotopic signal from it will not bias the δD. The 13 samples that contain chlorite form an array with similar $\delta^{18}O$ and highly variable δD values and represent some of the outliers (Table S3). Because of the likely detrital origin of chlorite, these samples are excluded from further calculations and from the figures. Samples from the first 170 m of the stratigraphic column preserve more negative δD values than the other samples, while the samples from the top 400 m of the sedimentary column (SB77-SB87) preserve more positive $\delta^{18}O$ values. The remaining samples (SB13-SB74), from ~170 to

~1400 m (between ~6.7-4.8 Ma, Fig. 3), form a tight cluster. The mean isotopic composition of clay in this group is $\delta^{18}O$ =12.4 ± 0.4‰ (1σ) and δD = -85.3 ± 2.2‰ (1σ).

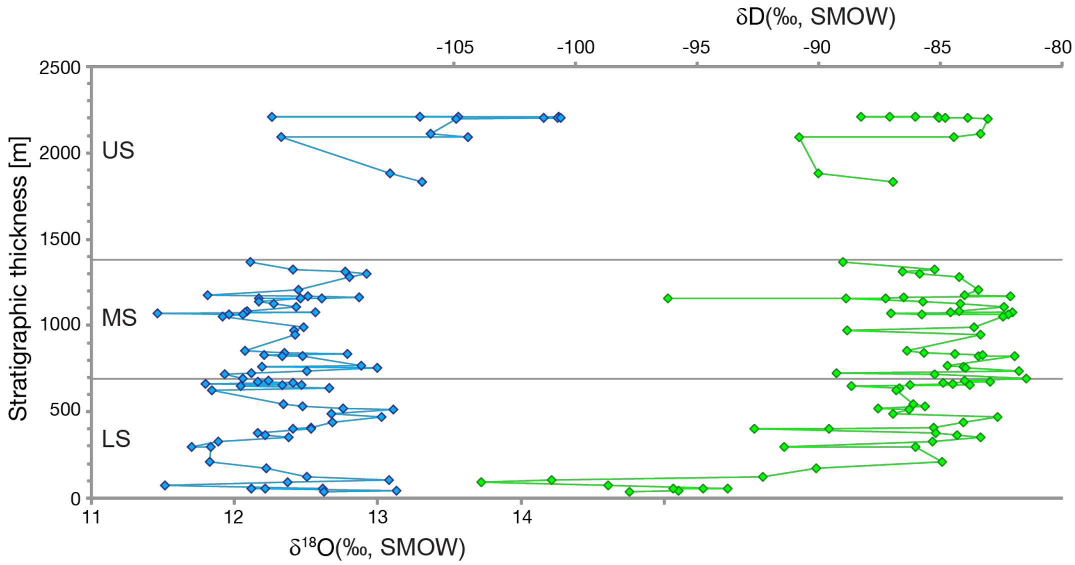

Figure 5. Isotopic composition of clays vs. their stratigraphic depth. Blue: $\delta^{18}O$, green: δD.

4.3 Isotopic composition of local meteoric water

Stable isotope composition of modern meteoric water samples is shown in Figure 6. On average, the $\delta^{18}O$ lapse rate is ~-0.25‰ per 100 m hypsometric basin elevation change, similar to empirical data for the central Himalayan front [*Garzione et al*., 2000; -0.23‰ to -0.35‰/100 m), eastern Tibet [*Hren et al*., 2009; -0.29‰/100 m] and a global calibration [*Poage and Chamberlain*, 2001; -0.28‰/100 m). The isotopic composition of meteoric water at the 100 m is estimated based on linear extrapolation (defined using an ordinary least squares regression) of isotopic composition vs. mean basin elevation as $\delta^{18}O$ = -4.5 +2.2/-1.2‰, δD = -33.8+16/-8‰. The local meteoric water line (LMWL) of eastern Bhutan Himalaya is defined using an ordinary least squares regression (Fig. 7). Its slope is slightly lower than that of the global meteoric water line (GMWL [*Craig*, 1961]); $\delta D = 7.24 \times \delta^{18}O - 0.97$ ($R^2 = 0.9$) vs. $\delta D = 8.20 \times \delta 18O + 11.27$ [*Rozanski et al.*, 1993].

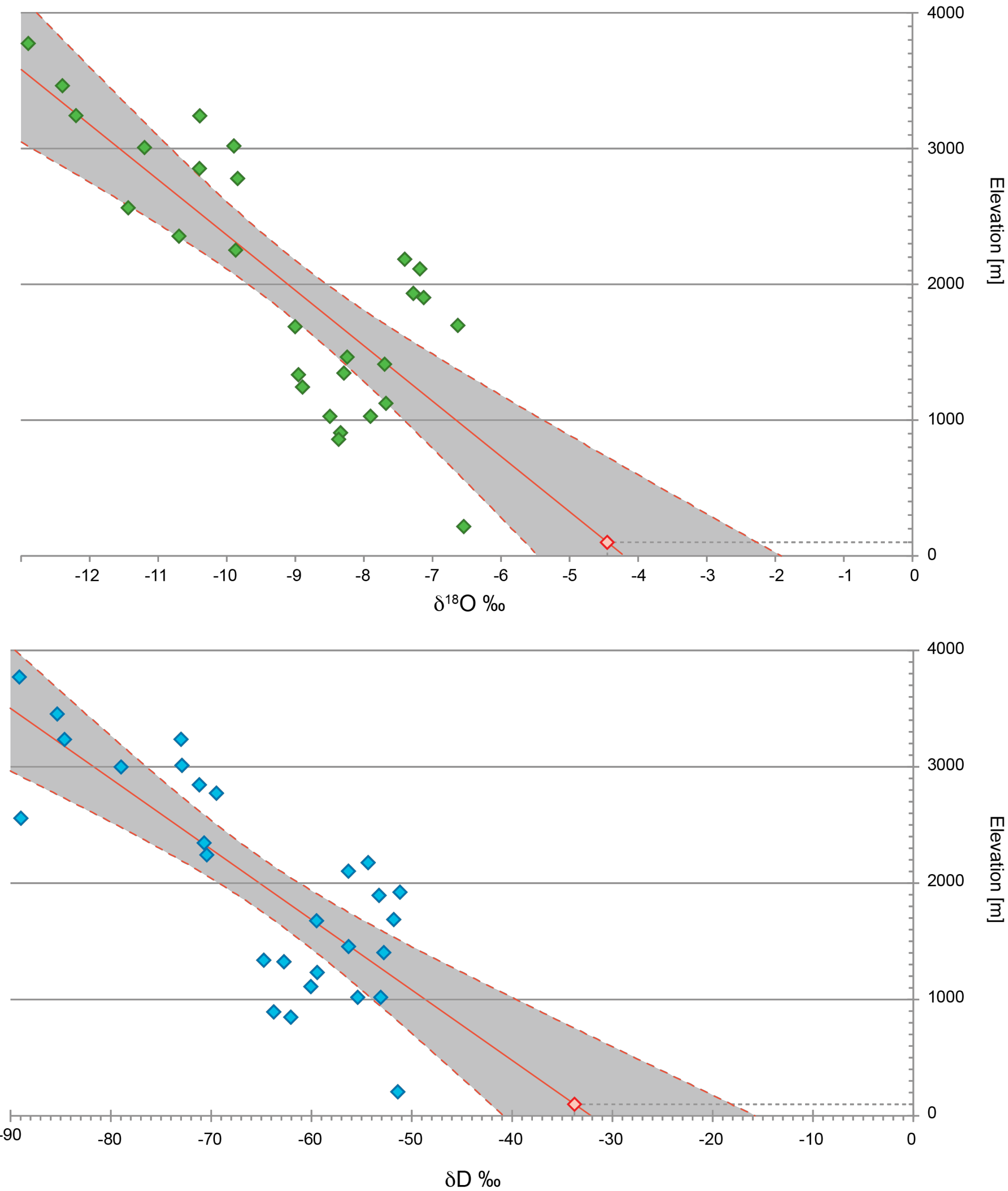

Figure 6. Isotopic composition of modern stream water vs. mean catchment elevation above sea level. Samples were collected between 26.8 and 27.6 °N. The continuous straight line is the linear best fit and dashed curved lines are the 2σ. Red symbols indicate the predicted mean isotopic composition of meteoric water at 100 m, the current elevation of the foreland basin at the latitude of Samdrup Jongkhar.

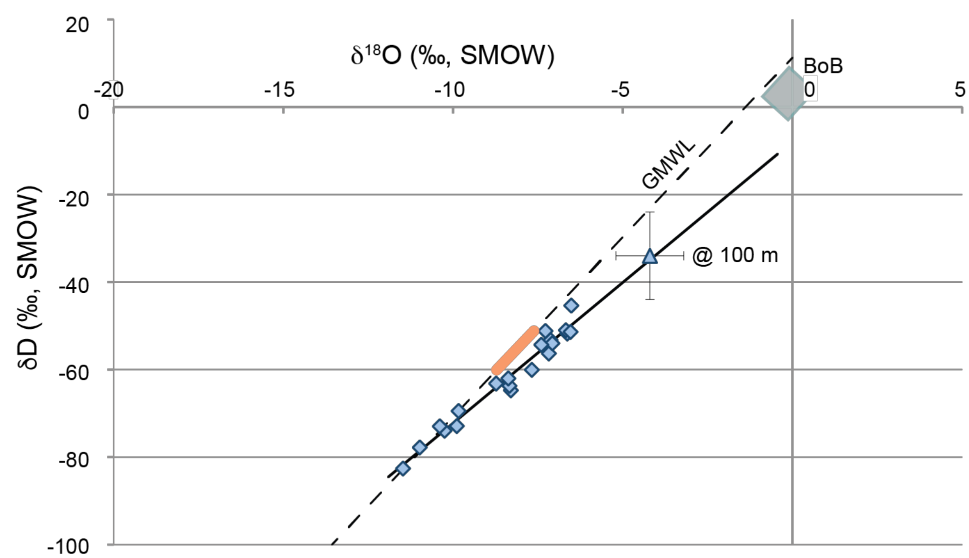

Figure 7. Oxygen and hydrogen isotopic composition of river waters. Dashed black line is the Global Meteoric Water Line (GMWL, [*Craig*, 1961]). Blue diamonds are measurements of the isotopic composition of stream water in eastern Bhutan (this study). Continuous black line is the Local Meteoric Water Lines (LMWL) for the stream waters from the eastern Bhutan Himalayas. The blue triangle is the isotopic composition of stream waters at 100 m elevation estimated from the isotopic value elevation linear regression (see Fig. 6). The error bars are 1σ uncertainties at that elevation. The blue rectangle is the range of isotopic compositions of sea-water in the Bay of Bengal (BoB, [Achyuthan et al., 2013]). Thick orange line is the range of values calculated for the palaeo-meteoric water in equilibrium with the pedogenic clays (see Fig. 8, and related text).

5. Discussion

5.1. Stable isotope composition of palaeosol clays as palaeoenvironmental proxies

In palaeosols, the clay fraction can represent a mixture of detrital, pedogenic, and burial authigenic clays, among which diagenetically altered pedogenic clays. Pedogenic clay minerals form in or close to oxygen isotopic equilibrium with the environment of formation [*Lawrence and Taylor*, 1972; *Savin and Epstein*, 1970; *Savin and Hsieh*, 1998]. Isotopic studies of clays thus yield useful information about climatic and pedogenic conditions during the time they formed [*Mix and Chamberlain*, 2014; *Rosenau and Tabor*, 2013; *Stern et al.*, 1997; *Tabor and Montañez*, 2005; *Tabor et al.*, 2002; *Vitali et al.*, 2002].

The isotopic data tightly cluster, rather than spread along the water line. This suggests that the pedogenic clays did not form at different elevations and wash in from the paleo-drainage. While it is possible that all of the clays were chemically and isotopically altered from their original compositions during burial and diagenesis, or that pedogenic clays from a given palaeosol may be composed of several different fractions that crystallised under different climatic regimes during soil development, we suggest that the bulk of clays preserved in these paleosols were formed *in situ*. We did not observe diagenetic processes such as cementation and mineral dissolution. Although there is likely detrital illite, it is most likely a weathering product that is washed in from the weathering in the catchment. Since the clays in a sample were formed at different places within the catchment, the paleo-meteoric water isotopic composition calculated from the clay $\delta^{18}O$ and δD values may be considered as average palaeoenvironmental conditions that persisted during weathering, pedogenesis and/or isotopic equilibration with meteoric waters during burial. We interpret the isotopic composition of clays as a combined signature that records the water isotopic signature that characterizes the integrated catchment.

5.2. Clay formation

The isotopes are most depleted in Unit 1 when the depositional environment was brackish or more likely to be influenced by brackish water. Thus, the switch to running water would cause stable isotope values to change in the opposite direction than observed. Both smectite and kaolinite result from intense terrain weathering under tropical to subtropical conditions. Kaolinite, as a pedogenic clay mineral, is favoured by acidic conditions and is unlikely to form in submerged, alkaline waters [*Gastuche and De Kimpe*, 1961]. While smectite is promoted by poor drainage (e.g. in low-lying areas) and contrasting wet/dry seasonality, kaolinite is favoured by well-drained areas of high, non-seasonal rainfall and is formed by extensive chemical weathering promoted by high rainfall and leaching [*Gastuche and De Kimpe*, 1961; *Robert and Chamley*, 1991; *Robert and Kennett*, 1994]. All of these conditions are consistent with the rainfall and temperature conditions of the study area and the complete lack of carbonate concretions in the sediments. Previous studies on clay minerals from Siwalik sediments have demonstrated that smectite is pedogenic rather than detrital [*Quade et al*., 1989; *Stern et al*., 1997] and that it predominantly forms during summer monsoon rainfalls [*Quade et al*., 1989].

In the Lower and Middle Siwaliks of eastern Bhutan, vitrinite reflectance (R_0) values of ~0.3-0.5% correspond to temperatures of ~ 60-85 °C [our work, *Coutand et al.*, 2016]. Based on this evidence, pedogenesis and the onset of diagenesis (compaction, but absence of cementation and mineral dissolution) are considered to be the dominant processes responsible for the palaeosol clay $\delta^{18}O$ and δD values reported in this study. The studied clays are therefore not strictly pedogenic, according to their temperature record, as they are likely isotopically altered by meteoric groundwater during shallow burial, and are therefore referred to as authigenic.

5.3. Isotopic composition of the palaeo-meteoric water

To interpret the isotopic composition of clays for palaeoclimate investigation, one must calculate the isotopic composition of the waters involved in transforming the initial minerals into authigenic clays. Meteoric water in equilibrium with authigenic clay minerals has a different isotopic composition than that of the clay minerals because of dissimilar fractionation processes for different isotopes and minerals.

However, all the samples consist of mixture of clays, the mean mineralogical composition of samples between 170 and 1400 m is kaolinite 45 wt. %, smectite 25 wt. % and illite 25 wt.%. The three minerals have different water-clay fractionation factors. For oxygen, the illite 1000 lnα value at 40 °C is 20.6‰, for kaolinite is 21.4 ‰ and for smectite is 22 ‰ according to *Sheppard and* Gilg (1996). For hydrogen, at 40°C the 1000 lnα value for smectite is -37 ‰ from *Yeh* (1980), for kaolinite it is -30‰ according to *Sheppard and Gilg* (1996). The difference between these values is small, therefore for the end members the difference in calculated isotopic composition of paleo-meteoric water would be smaller than the spread of the data, and any variation in mineral abundance is only going to have a small effect. The paleo-meteoric water isotopic compositions can be calculated from the isotopic compositions of clay mixture (e.g., [*Bauer et al.*, 2016; *Rosenau and Tabor*, 2013]). Because of the similar mineralogical composition to their samples we have adopted the approach by [*Rosenau and Tabor*, 2013] using the hydrogen clay mixture-water fractionation equation:

$$1000 \ln {}^{D}\alpha_{mix-W} = -2.2 \cdot 10^{6} T^{-2} - 10.64 \tag{1}$$

and the oxygen clay mixture-water fractionation equation:

$$1000 \ln {}^{18}\alpha_{mix-W} = 2.83 \cdot 10^{6} T^{-2} - 7.17 \tag{2}$$

where α is the fractionation factor, and *T* is the temperature in K. For the calculations, we use the mean isotopic composition of clays (between 170 and 1400 m, cf. Fig. 5): $\delta^{18}O = 12.43 \pm 0.42$‰ and δD -85.29 ± 2.17‰. The mean meteoric water compositions in equilibrium with our clay mixture for temperatures of 10-90 °C define a line that intersects the modern GMWL at $\delta^{18}O = -7.8 \pm 0.4$ ‰ and δD = -53.2 ± 2 ‰ (Figure 8), which is interpreted as the mean isotopic composition of palaeo-meteoric water in equilibrium with the clays. Conversely, the intersection on the temperature line indicates that the mean temperature of the palaeo-meteoric water was ~48 °C.

To estimate the sensitivity of these results on mineral composition we compare them to the values that would be obtained for a pure kaolinite. Equations 1 and 2 are very close in form to the hydrogen kaolinite-water fractionation equation [*Sheppard and Gilg*, 1996]:

$$1000 \ln {}^{D}\alpha_{K-W} = -2.2 \cdot 10^{6} T^{-2} - 7.7 \tag{3}$$

and the oxygen kaolinite-water fractionation equation [*Sheppard and Gilg*, 1996]:

$$1000 \ln {}^{18}\alpha_{K-W} = 2.76 \cdot 10^{6} T^{-2} - 6.75 \tag{4}$$

Using these equations and the mean composition of the clay minerals, the meteoric water compositions in equilibrium with kaolinite for temperatures of 10-90 °C define a line that intersects the modern GMWL at $\delta^{18}O$ = -8.2 ± 0.4 ‰ and δD = -56 ± 2 ‰ (Figure 8a), which is interpreted as the mean isotopic composition of palaeo-meteoric water in equilibrium with the kaolinite. Conversely, the intersection on the temperature line indicates that the mean temperature of the palaeo-meteoric water was ~45 °C. Considering the range of parameters in equations 1-4 the isotopic and temperature values for pure kaolinite are the minimum and the errors on the $\delta^{18}O$ and δD caused by variable mineral composition are on the order of ± 0.4 ‰ and ± 2 ‰ respectively.

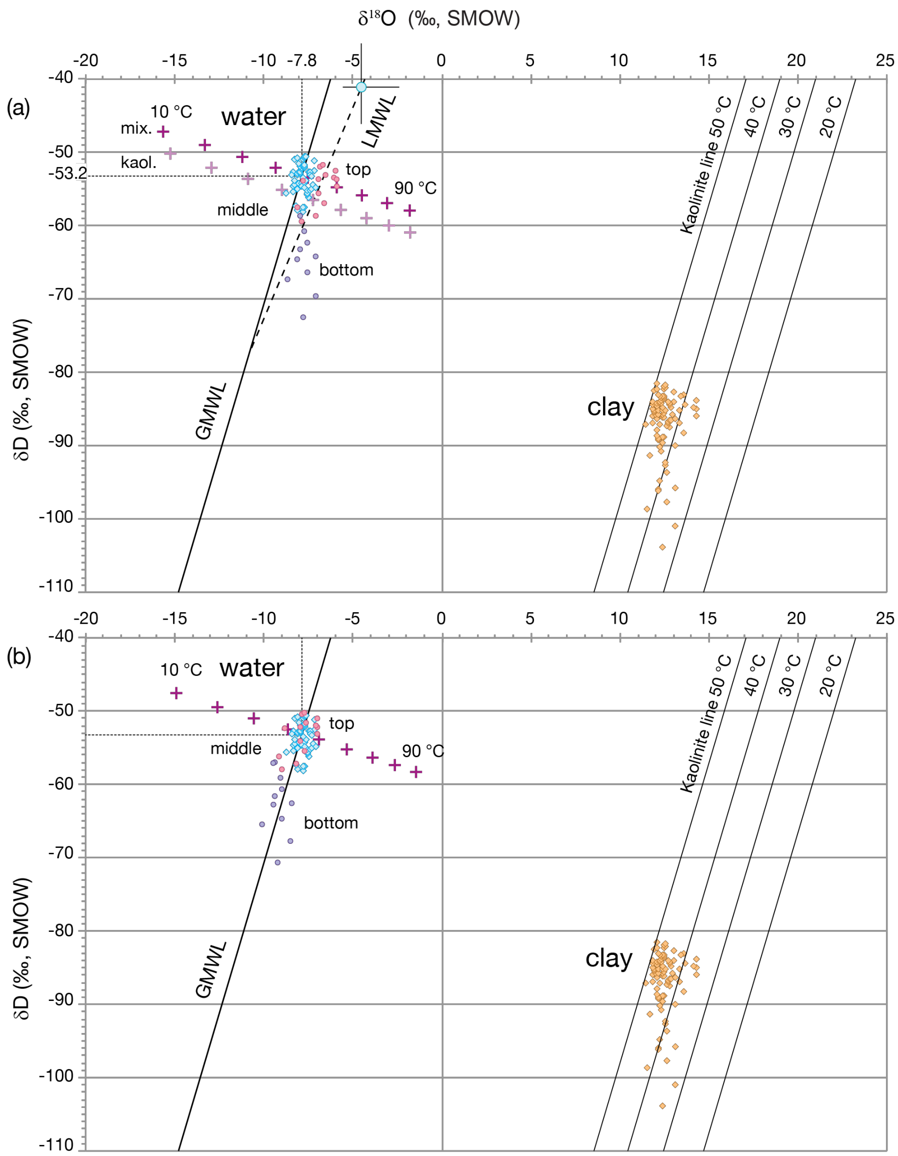

Figure 8. Bivariate plot of δ^{18}O vs. δD showing composition of clay samples (brown) and the expected water of formation (blue). Kaolinite line (δD=7.55*δ^{18}O-219; [*Sheppard and Gilg*, 1996] represents the isotopic composition of kaolinite formed in equilibrium with meteoric water at 20, 30, 40 and 50 °C [*Savin and Epstein*, 1970]. The majority of clay isotopic data suggests clays formed at temperatures of ~45 °C. The mean meteoric water compositions in equilibrium with kaolinite and a clay mixture for temperatures of 10-90 °C are represented as purple and pale purple crosses, respectively. (a) Calculated isotopic composition of the palaeo-water in

equilibrium with the clay minerals at 48 °C. Purple: samples from the bottom 170 m within Unit 1. Blue: samples from the middle part (Units 1-3). Pink: samples from the top 400 m of the stratigraphic section (Unit 4). Blue circle with error bars shows the isotopic composition of modern water at the foreland basin elevation. (b) Calculated isotopic composition of the palaeo-water in equilibrium with the clay minerals assuming different temperatures of formation/isotopic equilibration: 37.2 °C for the bottom, 45.2 °C for the middle, and 38.9 °C for the top of the section. These three values represent average temperatures for the same sections calculated using equation 5 (Fig. 9).

Assuming that the clay minerals formed in equilibrium with surface water and shallow groundwater of meteoric origin (two of which have similar stable isotope composition), the kaolinite-water fractionation factors of opposing slopes (equations 3 and 4) can be combined with the global meteoric water relationship to calculate temperatures of paleo-meteoric water for each sample ([*Mix et al.*, 2016]; and references therein):

$$3.0350 \cdot 10^{6} T^{-2} = \delta^{18}O_K - 0.1250\delta D_K + 7.0375 \tag{5}$$

where T is the absolute temperature in K. We use the modern meteoric water relationship to solve for the temperature assuming that the water they formed from falls on the GMWL.

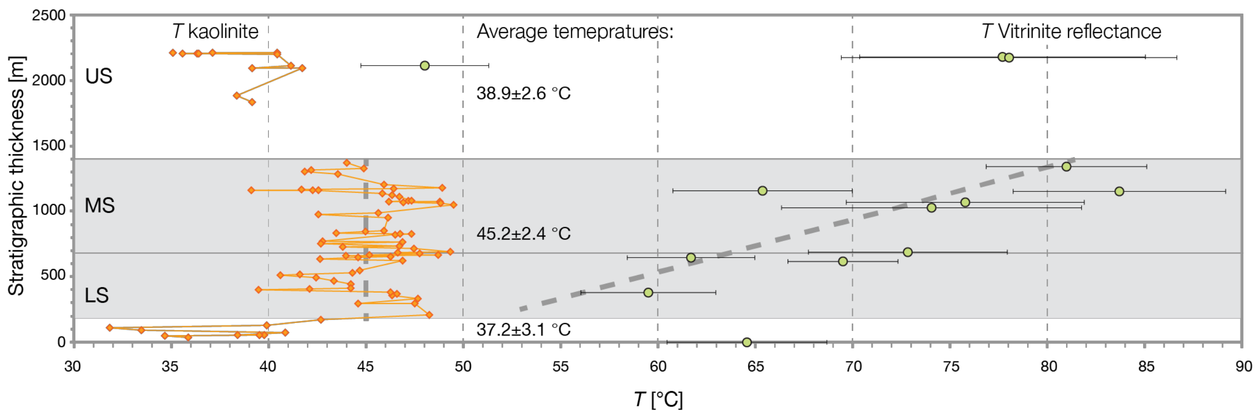

Figure 9. Calculated paleotemperatures. Orange symbols indicate temperature of isotopic equilibration between palaeo-meteoric water and clay minerals. This calculation assumes all the clay minerals are kaolinite and uses equation (5) by *Mix et al.* [2016]. The temperatures range between ~30 and ~ 50 °C, but average 38.9±2.6 °C for the bottom, 45.2±2.4 °C for the middle, and 38.9±2.6 °C for the top of the section. Errors are estimated to ± 3 °C but the error bars are omitted for clarity. Green symbols indicate peak burial temperatures inferred from vitrinite reflectance (*Coutand et al.* [2016] and our new data). Dashed grey lines are the trends for the two temperature sets over the stratigraphic section between 170 and 1400 m.

There are two alternative explanations for the trends of calculated stable isotope data in paleo-meteoric water. (1) The water isotopic compositions are defined by GMWL, therefore, we use the clay $\delta^{18}O$ and δD values to explain variance in measured values as a function of formation temperature. This places all samples between 30-50 °C suggesting that the clays probably formed or equilibrated with the meteoric water during shallow burial. The calculated temperatures are somewhat lower for the bottom 170 m and top 400 m of the sedimentary section (Figs. 8b and 9). Alternatively, (2) the difference in the calculated paleo-water composition and temperature can be explained by the difference in clay mineralogy and associated fractionation factors which would yield varying temperature estimates depending on the used mineral-water equation. We have however shown (section 5.3) that that the fractionation factors for the three clay minerals are fairly similar, the kaolinite yields lowest values and any variation in clay mixture would have small effect (Figure 8a). Accordingly, we opted for the former interpretation.

Currently, the mean annual temperature across the Himalaya decreases with elevation from 25 °C in the foreland ([*Ohsawa*, 1991], NOAA data for the town of Guwahati, ftp://dossier.ogp.noaa.gov/GCOS/WMO- Normals/RA-II/IN/42410.TXT), following an atmospheric lapse rate of 6 °C/km [*Naito et al.*, 2006]. The modern average annual temperature of the Himalayan foreland is believed to have remained constant since deposition of the Siwalik sediments, even with the northward drift of India during the last 7 Ma [*Quade et al.*, 2011]. Temperature of 48 °C could be reached with a burial depth of about 650-1000 m, considering the geothermal gradient in the foreland basins of the region of 20-30 °C/km ([*Biswas et al.*, 2007] and references therein). Once formed, clays are resistant at surficial temperatures to subsequent oxygen isotopic exchange with the environment in the absence of mineralogical reaction [*Savin and Epstein*, 1970]. This would suggest that the bulk of the clays were formed or recrystallized between the surface and depth of up to one kilometre.

The composition of rainwater in New Delhi is $\delta^{18}O$ = -5.41‰, δD = -34.06‰ (IAEA/WMO, 2012). The groundwater in the plains between eastern Bhutan and the Brahmaputra valley records $\delta^{18}O$ = -5.54‰ and δD = -36.38‰ [*Verma et al.*, 2015], and we estimate the composition of meteoric waters to be $\delta^{18}O$ = -4.5 +2.2/-1.2‰, δD = -33.8+16/-8‰ at the level of the modern foreland basin in eastern Bhutan (~100 m). These isotopic compositions are identical within error. We are, therefore, confident that the calculated stable isotope composition of palaeo-meteoric waters at ~1 km depth is similar to the isotopic composition of palaeo-waters at the surface of the Siwalik sedimentary basin. Consequently, the difference between the isotopic composition of meteoric waters reflects the magnitude of change in environmental parameters.

5.4. Causes of changes in isotopic composition of foreland meteoric water

In the following section, we discuss the five physical factors that can cause a change in $\delta^{18}O$ values across the geological time-scale: temperature, elevation, latitude, distance from the shore, and precipitation volume [*Dansgaard*, 1964].

First, the global palaeoclimate record based on benthic foraminifera shows an overall increase in $\delta^{18}O$ from the Middle Miocene to the Pliocene [*Zachos et al.*, 2001]. This increase in $\delta^{18}O$ within the oceans corresponds to a period of global cooling and an increase in ice volume. In addition, the global Pliocene-Pleistocene stack of benthic $\delta^{18}O$ data [*Lisiecki and Raymo*, 2005] suggests the presence of a deep-water temperature signal from 2.7 to 1.6 Ma. The global decrease in temperature, and related increase in $\delta^{18}O$ by ~1‰ since 4-5 Ma (using the data from *Lisiecki and Raymo* [2005]) could, therefore, account for part of the ~3.3‰ increase in calculated palaeo-meteoric water $\delta^{18}O$ values calculated in this study.

Second, the isotopic composition of meteoric water changes with elevation [*Drever*, 1997; *Poage and Chamberlain*, 2001; *Quade et al.*, 2011]: both $\delta^{18}O$ and δD values decrease with decreasing elevation. However, the elevation of the Neogene Siwalik sedimentary basin could not have been higher than the modern foreland basin (i.e. Brahmaputra valley) at ~100 m a.s.l.

Thus, the foreland basin elevation decrease cannot account for the observed variations in the isotopic composition of meteoric water.

Third, $\delta^{18}O$ and δD values are lower at higher latitudes because of the decreasing temperature and of the increasing degree of 'rain-out' [*Drever*, 1997]. Latitudinal changes in an area (e.g., a sedimentary basin) due to the displacement of crustal plates can, therefore, generate $\delta^{18}O$ changes [*Drever*, 1997]. India has moved northward by ~24° over the past 52 Ma [*Huang et al.*, 2015], but only by 4.5° over the past 11 Ma. Accordingly, because of the 320 km northward displacement of India between the time of deposition of the oldest Siwalik sediments (~7 Ma) to the present, the $\delta^{18}O$ value of meteoric water would have decreased on the order of 0.3‰, using the polynomial fit to the global variations in isotopes in precipitation derived by [*Bowen and Wilkinson*, 2002] and assuming a constant distance from the ocean shore.

Fourth, we know that the sediments from units 1 and 2 were deposited in marginal marine river- and wave-influenced deltaic systems, whereas units 3 and 4 correspond to sediments of alluvial systems [*Coutand et al.*, 2016; *Najman et al.*, 2016], hence the distance to the shore has progressively increased. The precipitation at the centre of a large land mass or continent. usually has lower $\delta^{18}O$ and δD values, a phenomenon known as the 'continental effect' [*Dansgaard*, 1964; *Lachniet*, 2009; *Rozanski et al.*, 1993] but we do not observe this effect in calculated $\delta^{18}O$ values of paleo-meteoric water (they should be more positive), while the δD values are significantly more negative at the base of the section, opposite to what would be expected for samples located closer to coastal areas.

Finally, at low latitudes and in regions affected by monsoonal precipitation, the isotopic composition of precipitation may be more dominated by the amount of precipitation rather than by previously discussed factors [*Blisniuk and Stern*, 2005]. The fifth factor to consider is thus the amount of precipitation and its effect on $\delta^{18}O$ values, also known as the 'rainout effect' or 'amount effect' [*Dansgaard*, 1964]. The initial liquid phase of rain is enriched in ^{18}O and ^{2}H compared to subsequent phases of precipitation. Consequently, during rainfall events, the water becomes progressively depleted in ^{18}O and ^{2}H, leading to more fractionated or lower $\delta^{18}O$ values with higher precipitation levels [*Hoefs*, 2008]. If all the other four factors were held constant while precipitation decreased, the $\delta^{18}O$ value of meteoric water would increase. According to this effect, the period of monsoon intensification at approximately 7-8 Ma [*Quade et al.*, 1989] would have caused a decrease in the $\delta^{18}O$ values of meteoric water within regions affected by the monsoon due to higher precipitation and intense rainout. In contrast, from 2.7 Ma until recent times, the monsoon weakened due to global cooling, thereby increasing the $\delta^{18}O$ values of meteoric water [*Quade et al*., 1989]. As the global ice volumes increased, the ISM was affected by aridification, such that the strength decreased and evaporation from the land increased [*Thomas et al.*, 2002].

In addition, passage of a warm, moist air mass over a mountain like the Shillong Plateau (mean elevation 1600 m a.s.l.), and subsequent high precipitation on its windward, southern slopes would typically cause depleted rain on its leeward side—the "isotopic rain shadow" of [*Blisniuk and Stern*, 2005; *Poage and Chamberlain*, 2002]. Therefore, before uplift of the plateau, the meteoric water in Bhutan would have been ^{18}O and ^{2}H enriched compared to recent meteoric water compositions, keeping other factors constant.

As there are five principal factors that affect the isotopic composition of meteoric water, it would be difficult to identify a unique cause of the ~3.3‰ increase in the $\delta^{18}O$ values of meteoric water since isotopic equilibration of the Siwalik sediments. However, some factors are inferred to have less effect (elevation changes) or an opposite effect (latitudinal changes, distance from the shore) on the isotopic composition of authigenic clays, which may negate the $\delta^{18}O$ increase. Climate model studies test the response of $\delta^{18}O$ precipitation values to various atmospheric processes (e.g., [*Dayem et al.*, 2010; *Roe et al.*, 2016]. Models of the $\delta^{18}O$ values of meteoric water for New Delhi, taking into account a 14 °C drop in soil temperature, the northward drift of India by 10°, and a roughly 1‰ increase in the $\delta^{18}O$ value of sea-water due to global cooling and ice sheet formation, show that the $\delta^{18}O$ value of meteoric water in New Delhi would have remained constant over the past 50 Ma [*Quade et al.*, 2011]. Fully coupled comprehensive climate numerical experiments considering a realistic yet idealised palaeogeography and landscape, which retain the modern Himalayan topography at the estimated location of the suture, and set other elevations to zero [*Roe et al.*, 2016], also suggest that precipitation $\delta^{18}O$ values would have been significantly lower than modern values over the southward displaced Himalayas, while its immediate foreland would see no relative changes in isotopic composition. In addition, the Himalayan foreland basin elevation has remained constant at 0 to 100 m. Consequently, the only variable factors since the Late Miocene in eastern Bhutan are global cooling and the amount of precipitation.

5.5. Quantifying the amount effect

In this study, we estimate the composition of modern meteoric waters at $\delta^{18}O = -4.5\ +2.2/-1.2‰$, at the level of the foreland basin in eastern Bhutan (~100 m), and the mean isotopic composition of palaeo-meteoric water in equilibrium with clay minerals in the middle section of the Siwalik sediments at $\delta^{18}O = -7.8 \pm 0.4‰$. Part of the observed increase of $\delta^{18}O$ values of meteoric water above the lowest 170 m of the section (i.e. younger than ~7.2-6.7 Ma) can be explained by global cooling and ice volume changes [*Lisiecki and Raymo*, 2005] starting at approximately the same time. Consequently, to estimate the local climatic change, we subtract the ~1‰ $\delta^{18}O$ increase due to global cooling and ice volume increase from the total change in the isotopic record of ~3.3‰ $\delta^{18}O$ to arrive at ~ 2.5‰ $\Delta\delta^{18}O$. To interpret this observation in terms of precipitation variations with time, we make the following assumptions: (1) the $\delta^{18}O$ values are a valid proxy for monthly precipitation amounts [*Lachniet and Patterson*, 2006]; (2) the clay minerals preserve an integrated stable isotope signal of meteoric water in the catchment area; (3) the mean isotopic composition of the palaeo-meteoric water at shallow depth was in equilibrium with the Siwalik clay minerals; (4) the composition of stream waters within the eastern Bhutan Himalaya is representative of current meteoric waters in the foreland basin; and (5) the elevation and mean annual surface temperature of the Himalayan foreland basin have remained constant until the present. We apply the scale analysis by *Dayem et al.* [2010] to explore whether different amounts of local annual precipitation or different amplitudes of seasonal cycles (monsoon strengthening/weakening) can explain the difference between $\delta^{18}O$ in the clay record and modern $\delta^{18}O$ values. We use the empirical relationship between the monthly precipitation and monthly average $\delta^{18}O$ in New Delhi to estimate the change in annual precipitation required to produce the ~2.5‰ $\delta^{18}O$ difference. The difference, D, between a past and modern climate state is given by *Dayem et al.* [2010],

$$D = aP_0\left[\left(f_0 - 1\right) + \frac{1}{2}\left(\frac{f'^2}{f_0} - 1\right)\right] \tag{6}$$

where P_0 is the modern monthly precipitation, $a = \Delta\delta^{18}O/\Delta P$ is the slope of the best fit line, and f_0 and f' are factors that scale the annual mean and amplitude of seasonal variability, respectively. For the modern day $f_0 = f' = 1$.

To decrease the $\delta^{18}O$ values by 2.5‰ (between at 4.5 Ma and the present day), we estimate that the mean annual precipitation during deposition of the Siwalik sediments must have been ~2.5 times larger than today (at New Delhi). For comparison, a 1‰ decrease in $\delta^{18}O$ values due to global cooling would have caused 1.7 times higher precipitation in the past (Fig. 10, curve a). For the relative amount of summer to winter precipitation to increase sufficiently to cause a 2.5‰ or 1‰ decrease in the values, the mean annual precipitation must have been ~1.8 or 1.3 times larger, respectively, along the Himalayan front in our study area than at present (Fig. 10, curve b). Finally, changing the amplitude of the seasonal cycle cannot cause a decrease of the $\delta^{18}O$ value by as much as 1‰, given the upper limit of *f'* (Fig. 10, curve c).

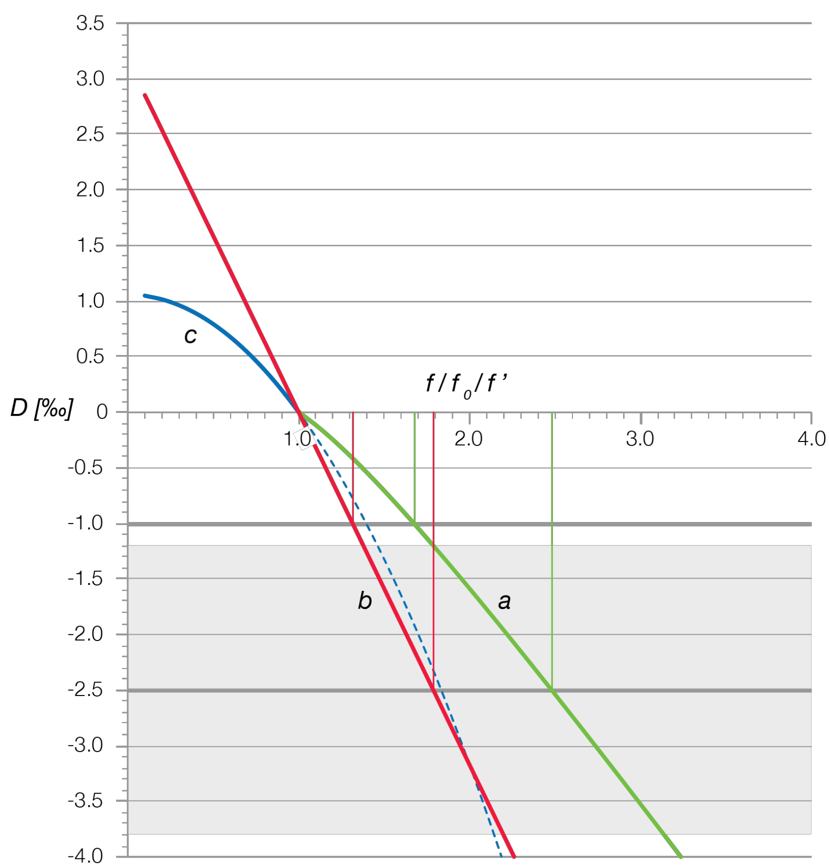

Figure 10. Calculated annual average precipitation-weighted $\delta^{18}O$ values relative to modern values for New Delhi, *D*, as a function of (a) mean annual precipitation amount f_0 holding $f'=1$; (b) $f=f_0=f'$, a case where the mean annual and seasonal amplitude of precipitation vary proportionally; and (c) the seasonal amplitudes f' holding $f_0=1$. For the modern day, $f_0=f'=1$. For a climate where mean annual precipitation is larger or smaller than present, $f_0>1$ or $f_0<1$. For a climate with wetter summers and drier winters (stronger monsoon) than present, $f'>1$, and for a climate with less seasonal variability (less monsoonal) than present, $f'<1$. Parameters values in equation 5, derived from 334 data points covering the period 1960-2012 (IAEA/WMO 2012), are a=-0.0178 ‰/mm/month, and P_0=119.02 mm/month. Grey area indicates the enrichment of modern waters in $\delta^{18}O$ by 3.3 ± 1.3‰ relative to the palaeometeoric waters.

5.6. Time of changes in isotopic composition of foreland meteoric water

The comparison of paleo-meteoric and modern meteoric waters suggests an increase in $\delta^{18}O$ by ~3.3 +2.2/-1.3‰ since the deposition of the Siwalik sediments at ~1400 m of the study section, i.e., since the period between 4.8 and 4.5 Ma. However, because the clay minerals formed or equilibrated with the meteoric water during burial, their isotopic composition was acquired when the sediments reached the corresponding depth, not at their stratigraphic age. According to the calculated sedimentation rates [*Coutand et al.*, 2016], sediments from the base of the section attained the depth of burial corresponding to 48 °C by 5.5 to 6.0 Ma for geothermal gradients of 20 and 30 °C/km, respectively (Fig. 11). Similarly, the sediments after which there is a change in isotopic composition of authigenic clay minerals, have the stratigraphic age of 4.8-4.5 Ma (cf. Figs 2 and 5) but attained the depth of burial corresponding to 48 °C by ~1.2-1.7 Ma for a geothermal gradient of 20 and 30 °C/km, respectively (Fig. 11). Hereafter, we shall refer to these stages as the "time of isotopic equilibration".

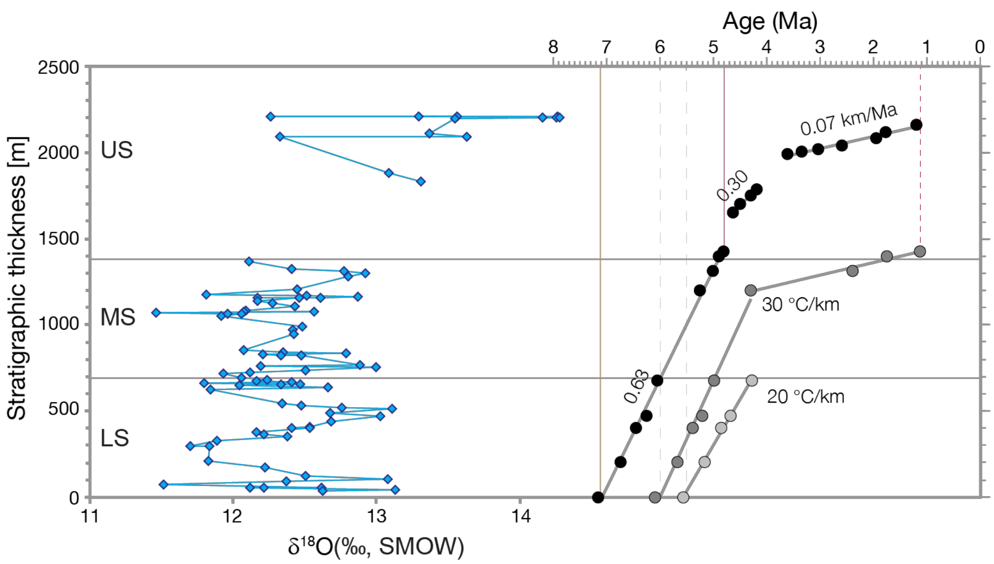

Figure 11. Estimate of the time of isotopic equilibration. In blue are the $\delta^{18}O$ values of the clays. Black dots are the age/depth points, which also provide the estimate of sediment accumulation rate (from *Coutand et al., 2016*). Dark grey are the estimates of time at which a stratigraphic point would attain the depth of 670 m (i.e., 48 °C according to the geothermal gradient of 30 °C). Pale grey are the estimates of time at which a stratigraphic point would attain the depth of 1000 m (i.e., 48 °C according to the geothermal gradient of 20 °C).

Because the most significant changes in isotopic composition of clays occur after the regional monsoon weakening at ~ 2.7 Ma, we propose that this decrease in mean annual precipitation in eastern Bhutan is due to the topographic uplift of the Shillong Plateau, causing strong orographic precipitation along its southern flank, and generation of a large rain shadow on its leeward side. The data from our study thus suggest that the effects of a rain shadow were established at ~1.2-1.7 Ma. This is consistent with initiation of plateau surface uplift in the

Pliocene [*Biswas et al.*, 2007; *Rosenkranz et al.*, 2018; *Govin et al*. 2018], and suggests that the Shillong Plateau attained sufficient elevation (~1500 m, e.g., [*Roe*, 2004]) to cause orographic rainout on its southern slope only after ~1.2-1.7 Ma. The Shillong Plateau is not the only factor affecting the change in precipitation distribution, as global cooling and consequential weakening of the monsoon could also account for a portion of the decrease in precipitation and increase in $\delta^{18}O$ values.

6. Conclusions

We analysed the oxygen and hydrogen isotopic composition of clay minerals found in the entire stratigraphic column of the Siwalik Group sediments in eastern Bhutan. The stratigraphic age of the sedimentary column has been constrained to ~7.2 to ~1.2 Ma. The mean $\delta^{18}O$ and δD values of clay mineral assemblages are 12.4 and -85.3, respectively. Taking in account the mineralogical composition of the clays, we calculated the stable isotope composition of the palaeo-meteoric water as $\delta^{18}O$= -7.8 ± 0.4‰ and δD =-53.2 ± 3‰, and the equilibration temperature of ~48 °C. Such a temperature could have been reached at a depth of ~1 km or less.

Furthermore, we constrained the LMWL for the eastern Himalayas in Bhutan, and the average isotopic composition of modern meteoric water at the elevation of the foreland basin is δD=7.24 ‰ and $\delta^{18}O$ = -0.97 ‰ (R^2 = 0.9). The modern $\delta^{18}O$ values are 3.3 ‰ more positive relative to the mean isotopic composition of meteoric water during deposition of the Siwalik sediments.

$\delta^{18}O$ and δD value changes have been interpreted with caution in terms of the amount effect. The most likely explanation for these more positive $\delta^{18}O$ values is a decrease in precipitation rate in the foreland and foothills of the eastern Himalayas. The most plausible cause for this is the orographic effect triggered by the surface uplift of the Shillong Plateau that focused extremely high amounts of precipitation on it southern slopes. In addition to the Shillong orographic barrier, global cooling and consequential weakening of the monsoon could also account for a portion of the decrease in precipitation and increase in the $\delta^{18}O$ values of meteoric water.

Of the three palaeoclimatic stages recorded in the stable isotopes of Siwalik clays, the first (~7.2-6.7 Ma) may be related to the shift at ~7 Ma towards more seasonal and overall drier climate in the western and central Himalaya [*Vögeli et al.*, 2017, and references therein], although this climatic change has not been observed in the eastern Himalaya on the base of carbon isotopes in organic matter [*Vögeli et al.*, 2017] or palynological assemblages [*Coutand et al.,* 2016]. The second palaeoclimatic stage, recorded in sediments ~6.7 to ~4.8 Ma old, shows constant isotopic values and therefore constant palaeoclimatic conditions. The subsequent increase in $\delta^{18}O$ values most plausibly records a decrease in mean precipitation rates associated with uplift of the Shillong Plateau. Because the isotopic equilibration of clay minerals was achieved at temperatures corresponding to sedimentary burial down to ~1000 m depths, climatic changes preserved in sediments younger than ~4.8-4.5 Ma have occurred after ~1.2-1.7 Ma. Although it surface uplift started after ~4-3 Ma, we suggest that the Shillong Plateau did not reach the threshold elevation required to produce a significant orographic barrier to Himalayan moisture until ~1.2 Ma.

Acknowledgments

Dedicated to Gwladys Govin.

Fieldwork was supported by the France-Stanford Foundation (IC), the Natural Sciences and Engineering Research Council of Canada (Discovery grant RGPIN 371671 to IC and RGPIN 04297 to DG) and the National Geographic Society (Scientific research grant 83118-07 to DG). DG and IC thank the Herbette Foundation and the Swiss National Foundation for financial support (visiting professorship grants) during the writing of the manuscript at the University of Lausanne. The work of LB for this publication is the IPGP contribution 3775. Shell fund at Dalhousie University provided the financial support to BC for her work visit to the University of Lausanne. Clay and water isotopic data are available in the Supporting Information and samples are available upon request to the corresponding author.

References

Achyuthan, H., R. Deshpande, M. Rao, B. Kumar, T. Nallathambi, K. Shashi Kumar, R. Ramesh, P. Ramachandran, A.S. Maurya, and S. K. Gupta (2013) Stable isotopes and salinity in the surface waters of the Bay of Bengal: Implications for water dynamics and palaeoclimate. *Marine Chemistry* 149, 51-62. doi.org/10.1016/j.marchem.2012.12.006.

Adams, B., K. Whipple, K. Hodges, and A. Heimsath (2016), In situ development of high-elevation, low-relief landscapes via duplex deformation in the Eastern Himalayan hinterland, Bhutan, *Journal of Geophysical Research: Earth Surface*, *121*. DOI:10.1002/2015JF003508.

Bauer, K. K., and T. W. Vennemann (2014), Analytical methods for the measurement of hydrogen isotope composition and water content in clay minerals by TC/EA, *Chemical Geology*, *363*, 229-240. doi.org/10.1016/j.chemgeo.2013.10.039.

Bauer, K. K., T. W. Vennemann, and H. A. Gilg (2016), Stable isotope composition of bentonites from the Swiss and Bavarian Freshwater Molasse as a proxy for paleoprecipitation, *Palaeogeography, Palaeoclimatology, Palaeoecology*, *455*, 53-64. doi.org/10.1016/j.palaeo.2016.02.002.

Biswas, S., I. Coutand, D. Grujic, C. Hager, D. Stöckli, and B. Grasemann (2007), Exhumation and uplift of the Shillong plateau and its influence on the eastern Himalayas: New constraints from apatite and zircon (U-Th-[Sm])/He and apatite fission track analyses, *Tectonics*, *26*(6), n/a-n/a. doi:10.1029/2007TC002125.

Blisniuk, P. M., and L. A. Stern (2005), Stable isotope paleoaltimetry: a critical review, *American Journal of Science*, *305*(10), 1033-1074. doi: 10.2475/ajs.305.10.1033.

Bookhagen, B., and D. W. Burbank (2010), Toward a complete Himalayan hydrological budget: Spatiotemporal distribution of snowmelt and rainfall and their impact on river discharge, *Journal of Geophysical Research*, *115*, F03019. doi:10.1029/2009JF001426.

Bowen, G. J., and B. Wilkinson (2002), Spatial distribution of $\delta^{18}O$ in meteoric precipitation, *Geology*, *30*(4), 315-318. http://dx.doi.org/10.1130/0091-7613(2002)030<0315:SDOOIM>2.0.CO;2.

Breitenbach, S. F. M., J. F. Adkins, H. Meyer, N. Marwan, K. K. Kumar, and G. H. Haug (2010), Strong influence of water vapor source dynamics on stable isotopes in precipitation observed in Southern Meghalaya, NE India, *Earth and Planetary Science Letters*, *292*(1-2), 212-220. https://doi.org/10.1016/j.epsl.2010.01.038.

Champagnac, J. D., P. Molnar, C. Sue, and F. Herman (2012), Tectonics, climate, and mountain topography, *Journal of Geophysical Research: Solid Earth*, *117*(B2). doi:10.1029/2011JB008348.

Coutand, I., Whipp, D.M., Grujic, D., Bernet, M., Fellin, M.G., Bookhagen, B., Landry, K.R., Ghalley, S., Duncan, C. (2014) Geometry and kinematics of the Main Himalayan Thrust and Neogene crustal exhumation in the Bhutanese Himalaya derived from inversion of multithermochronologic data. *Journal of Geophysical Research: Solid Earth* 119, 1446-1481. doi:10.1002/2013JB010891.

Coutand, I., L. Barrier, G. Govin, D. Grujic, C. Hoorn, Dupont-Nivet, Guillaume, and Y. Najman (2016), Late Miocene-Pleistocene evolution of India-Eurasia convergence partitioning between the Bhutan Himalaya and the Shillong Plateau: New evidences from foreland basin deposits along the Dungsam Chu section, eastern Bhutan, *Tectonics*, *35*(12), 2963–2994. doi:10.1002/2016TC004258.

Craig, H. (1961), Isotopic variations in meteoric waters, *Science*, *133*(3465), 1702-1703. DOI: 10.1126/science.133.3465.1702.

Dansgaard, W. (1964), Stable isotopes in precipitation, *Tellus*, *16*, 436–468. https://doi.org/10.3402/tellusa.v16i4.8993.

Dayem, K. E., P. Molnar, D. S. Battisti, and G. H. Roe (2010), Lessons learned from oxygen isotopes in modern precipitation applied to interpretation of speleothem records of paleoclimate from eastern Asia, *Earth and Planetary Science Letters*, *295*(1), 219-230. https://doi.org/10.1016/j.epsl.2010.04.003.

DeCelles, P., G. Gehrels, J. Quade, and T. Ojha (1998), Eocene-early Miocene foreland basin development and the history of Himalayan thrusting, western and central Nepal, *Tectonics*, *17*(5), 741-765. doi:10.1029/98TC02598.

Dettman, D. L., M. J. Kohn, J. Quade, F. Ryerson, T. P. Ojha, and S. Hamidullah (2001), Seasonal stable isotope evidence for a strong Asian monsoon throughout the past 10.7 my, *Geology*, *29*(1), 31-34. DOI: https://doi.org/10.1130/0091-7613(2001)029<0031:SSIEFA>2.0.CO;2.

Drever, J. I. (1997), Catchment mass balance, in *Geochemical processes, weathering and groundwater recharge in catchments*, edited by Ola M. Saether & Patrice de Caritat, Rotterdam ; Brookfield, Vt : Balkema, pp. 241-261.

Epstein, S., Mayeda, T.K. (1953) Variation of O^{18} content of waters from natural sources. *Geochimica and Cosmochimica Acta* 4, 213-224. https://doi.org/10.1016/0016-7037(53)90051-9.

Garzione, C.N., Quade, J., DeCelles, P.G. and English, N.B. (2000) Predicting paleoelevation of Tibet and the Himalaya from δ18O vs. altitude gradients in meteoric water across the Nepal Himalaya. *Earth and Planetary Science Letters*, 183(1-2), 215-229. https://doi.org/10.1016/S0012-821X(00)00252-1.

Gastuche, M., and C. De Kimpe (1961), La genese des minéraux argileux de la famille du kaolin. II-Aspect cristallin, paper presented at Genese et synthese des argiles. Colloque CNRS, Centre National des Recherches Scientifiques. 105(8), pp. 75-88.

Gonfiantini, R. (1978) Standards for stable isotope measurements in natural compounds. *Nature* 271, 534–536. doi:10.1038/271534a0.

Govin, G., Najman, Y., Copley, A., Millar, I., van der Beek, P., Huyghe, P., Grujic, D., and Davenport, J. (2018) Timing and mechanism of the rise of the Shillong Plateau in the Himalayan foreland. *Geology*. doi.org/10.1130/G39864.1.

Grujic, D., I. Coutand, B. Bookhagen, S. Bonnet, A. Blythe, and C. Duncan (2006), Climatic forcing of erosion, landscape and tectonics in the Bhutan Himalayas, *Geology*, *34*, 801–804. DOI: https://doi.org/10.1130/G22648.1.

Herman, F., D. Seward, P. G. Valla, A. Carter, B. Kohn, S. D. Willett, and T. A. Ehlers (2013), Worldwide acceleration of mountain erosion under a cooling climate, *Nature*, *504*(7480), 423-426. doi:10.1038/nature12877.

Hirschmiller, J., D. Grujic, B. Bookhagen, I. Coutand, P. Huyghe, J. L. Mugnier, and T. Ojha (2014), What controls the growth of the Himalayan foreland fold-and-thrust belt?, *Geology*, *42*(3), 247-250. DOI: https://doi.org/10.1130/G35057.1.

Hoefs, J. (2008), *Stable isotope geochemistry*, Springer Science & Business Media. DOI:10.1007/978-3-319-19716-6.

Hoorn, C., T. Ohja, and J. Quade (2000), Palynological evidence for vegetation development and climatic change in the Sub-Himalayan Zone (Neogene, Central Nepal), *Palaeogeography Palaeoclimatology Palaeoecology*, *163*(3), 133-161. https://doi.org/10.1016/S0031-0182(00)00149-8.

Huang, W., D. J. Hinsbergen, P. C. Lippert, Z. Guo, and G. Dupont-Nivet (2015), Paleomagnetic tests of tectonic reconstructions of the Indi-Asia collision zone, *Geophysical Research Letters*, *42*(8), 2642-2649. doi: 10.1002/2015GL063749.

IAEA/WMO (2012). Global Network of Isotopes in Precipitation. The GNIP Database. Accessible at: http://www.iaea.org/water

IAEA/WMO (2012). Global Network of Isotopes in Rivers. The GNIR Database. Accessible at: http://www.iaea.org/water

Kendall, C., and T. Coplen (2001), Distribution of oxygen-18 and deuterium in river waters across the United States, *Hydrological processes*, 15(7), 1363–1393, doi:10.1002/hyp.217.

Lachniet, M. S. (2009), Climatic and environmental controls on speleothem oxygen-isotope values, *Quaternary Science Reviews*, *28*(5-6), 412-432. https://doi.org/10.1016/j.quascirev.2008.10.021.

Lachniet, M. S., and W. P. Patterson (2006), Use of correlation and stepwise regression to evaluate physical controls on the stable isotope values of Panamanian rain and surface waters, *Journal of Hydrology*, *324*(1-4), 115-140. https://doi.org/10.1016/j.jhydrol.2005.09.018.

Lawrence, J., and H. Taylor (1972), Hydrogen and oxygen isotope systematics in weathering profiles, *Geochimica et Cosmochimica Acta*, *36*(12), 1377-1393. https://doi.org/10.1016/0016-7037(72)90068-3.

Licht, A., et al. (2014), Asian monsoons in a late Eocene greenhouse world, *Nature*, *513*(7519), 501-506. doi:10.1038/nature13704.

Lisiecki, L., and M. Raymo (2005), A Plio-Pleistocene stack of 57 globally distributed benthic $\delta^{18}O$ records, *Paleoceanography*, *20*, 522–533. doi:10.1029/2004PA001071.

Marechal, A., Mazzotti, S., Cattin, R., Cazes, G., Vernant, P., Drukpa, D., Thinley, K., Tarayoun, A., Le Roux-Mallouf, R., Thapa, B.B., Pelgay, P., Gyeltshen, J., Doerflinger, E., Gautier, S. (2016) Evidence of interseismic coupling variations along the Bhutan Himalayan arc from new GPS data. *Geophysical Research Letters* 43, 12,399-312,406. doi:10.1002/2016GL071163.

Mix, H. T., and C. P. Chamberlain (2014), Stable isotope records of hydrologic change and paleotemperature from smectite in Cenozoic western North America, *Geochimica et Cosmochimica Acta*, *141*, 532-546. https://doi.org/10.1016/j.gca.2014.07.008.

Mix, H. T., D. E. Ibarra, A. Mulch, S. A. Graham, and C. P. Chamberlain (2016), A hot and high Eocene Sierra Nevada, *Geological Society of America Bulletin*, *128*(3-4), 531-542. DOI: https://doi.org/10.1130/B31294.1.

Moore, D., and R. Reynolds (1997), *X-Ray-Diffraction and the Identification and Analysis of Clay Minerals*, 174 pp., Oxford University Press.

Naito, N., Y. Ageta, S. Iwata, Y. Matsuda, and R. Suzuki (2006), Glacier shrinkages and climate conditions around Jichu Dramo Glacier in the Bhutan Himalayas from 1998 to 2003, *Bulletin of Glaciological Research*, *23*, 51-61.

Najman, Y., L. Bracciali, R. R. Parrish, E. Chisty, and A. Copley (2016), Evolving strain partitioning in the Eastern Himalaya: The growth of the Shillong Plateau, *Earth and Planetary Science Letters*, *433*, 1-9. https://doi.org/10.1016/j.epsl.2015.10.017.

Ohsawa, M. (Ed.) (1991), *Life zone ecology of the Bhutan Himalaya. II*, 249 pp., Laboratory of Ecology, Chiba University, Japan.

Poage, M. A., and C. P. Chamberlain (2001), Empirical relationships between elevation and the stable isotope composition of precipitation and surface waters: considerations for studies of paleoelevation change, *American Journal of Science*, *301*(1), 1-15. doi: 10.2475/ajs.301.1.1.

Poage, M. A., and C. P. Chamberlain (2002), Stable isotopic evidence for a Pre-Middle Miocene rain shadow in the western Basin and Range: Implications for the paleotopography of the Sierra Nevada, *Tectonics*, *21*(4). doi:10.1029/2001TC001303, 2002.

Quade, J., T. E. Cerling, and J. R. Bowman (1989), Development of Asian monsoon revealed by marked ecological shift during the latest Miocene in northern Pakistan, *Nature*, *342*(6246), 163-166. doi:10.1038/342163a0.

Quade, J., D. O. Breecker, M. Daeron, and J. M. Eiler (2011), The paleoaltimetry of Tibet: An isotopic perspective, *American Journal of Science*, *311*(2), 77-115. doi: 10.2475/02.2011.01.

Quade, J., J. M. L. Cater, T. P. Ojha, J. Adam, and T. M. Harrison (1995), Late Miocene environmental change in Nepal and the northern Indian subcontinent: Stable isotopic evidence from paleosols, *Geological Society American Bulletin*, *107*(12), 1381-1397.

Roe, G. H. (2004), Orographic precipitation, *Annual Review Earth Planetary Sciences*, *33*, 645-671. DOI: https://doi.org/10.1130/0016-7606(1995)107<1381:LMECIN>2.3.CO;2.1.

Roe, G. H., Q. Ding, D. S. Battisti, P. Molnar, M. K. Clark, and C. N. Garzione (2016), A modelling study of the response of Asian summertime climate to the largest geologic forcings of the past 50 Ma, *Journal of Geophysical Research: Atmospheres*, *121*. 5453–5470, doi:10.1002/2015JD024370.

Robert, C., and H. Chamley (1991), Development of early Eocene warm climates, as inferred from clay mineral variations in oceanic sediments, *Global and Planetary Change*, *3*(4), 315-331. https://doi.org/10.1016/0921-8181(91)90114-C.

Robert, C., and J. P. Kennett (1994), Antarctic subtropical humid episode at the Paleocene-Eocene boundary: Clay-mineral evidence, *Geology*, *22*(3), 211-214. DOI: https://doi.org/10.1130/0091-7613(1994)022<0211:ASHEAT>2.3.CO;2.

Rosenau, N. A., and N. J. Tabor (2013), Oxygen and hydrogen isotope compositions of paleosol phyllosilicates: Differential burial histories and determination of Middle–Late Pennsylvanian low-latitude terrestrial paleotemperatures, *Palaeogeography, Palaeoclimatology, Palaeoecology*, *392*, 382-397. https://doi.org/10.1016/j.palaeo.2013.09.020.

Rosenkranz, R., T. Schildgen, H. Wittmann, and C. Spiegel (2018) Coupling erosion and topographic development in the rainiest place on Earth: Reconstructing the Shillong Plateau uplift history with in-situ cosmogenic ^{10}Be. *Earth and Planetary Science Letters* 483, 39-51. https://doi.org/10.1016/j.epsl.2017.11.047

Rozanski, K., L. Araguás-Araguás, and R. Gonfiantini (1993), Isotopic patterns in modern global precipitation, *Climate change in continental isotopic records*, 1-36. DOI: 10.1029/GM078p0001.

Royal Government of Bhutan (2017) Statistical Yearbook of Bhutan 1988-2017. National Statistics Bureau, www.nsb.gov.bt, Accessed January 2018.

Rumble, D.I., Hoering, T.C. (1994) Analysis of oxygen and sulfur isotope ratios in oxide and sulfide minerals by spot heating with a carbon dioxide laser in a fluorine atmosphere. *Accounts of Chemical Research* 27, 237-241. DOI: 10.1021/ar00044a004.

Ryan, W. B. F., S. M. Carbotte, J. O. Coplan, S. O'Hara, A. Melkonian, R. Arko, R. A. Weissel, V. Ferrini, A. Goodwillie, F. Nitsche, J. Bonczkowski, R. Zemsky (2009), Global Multi-Resolution Topography synthesis, *Geochemistry Geophysics Geosystems*, *10*, Q03014. doi:10.1029/2008GC002332.

Savin, S. M., and S. Epstein (1970), The oxygen and hydrogen isotope geochemistry of clay minerals, *Geochimica et Cosmochimica Acta*, *34*(1), 25-42. https://doi.org/10.1016/0016-7037(70)90149-3.

Savin, S. M., and J. C. C. Hsieh (1998), The hydrogen and oxygen isotope geochemistry of pedogenic clay minerals: principles and theoretical background, *Geoderma*, *82*, 227-253. https://doi.org/10.1016/S0016-7061(97)00103-1.

Sheppard, S., and H. Gilg (1996), Stable isotope geochemistry of clay minerals, *Clay Minerals*, *31*(1), 1-24. DOI: https://doi.org/10.1180/claymin.1996.031.1.01.

Singer, J., Kissling, E., Diehl, T., Hetényi, G. (2017) The underthrusting Indian crust and its role in collision dynamics of the Eastern Himalaya in Bhutan: Insights from receiver function imaging. *Journal of Geophysical Research: Solid Earth* 122, 1152-1178. DOI: 10.1002/2016JB013337.

Sharp, Z. (1990) A laser-based microanalytical method for the in situ determination of oxygen isotope ratios of silicates and oxides. *Geochimica et Cosmochimica Acta* 54, 1353–1357. https://doi.org/10.1016/0016-7037(90)90160-M.

Stern, L. A., C. P. Chamberlain, R. C. Reynolds, and G. D. Johnson (1997), Oxygen isotope evidence of climate change from pedogenic clay minerals in the Himalayan molasse, *Geochimica et Cosmochimica Acta*, *61*(4), 731-744. https://doi.org/10.1016/S0016-7037(96)00367-5.

Tabor, N. J., and I. P. Montañez (2005), Oxygen and hydrogen isotope compositions of Permian pedogenic phyllosilicates: Development of modern surface domain arrays and implications for paleotemperature reconstructions, *Palaeogeography, Palaeoclimatology, Palaeoecology*, *223*(1), 127-146. https://doi.org/10.1016/j.palaeo.2005.04.009.

Tabor, N. J., and T. S. Myers (2015), Paleosols as indicators of paleoenvironment and paleoclimate, *Annual Review of Earth and Planetary Sciences*, *43*, 333-361. https://doi.org/10.1146/annurev-earth-060614-105355.

Tabor, N. J., I. P. Montanez, and R. J. Southard (2002), Paleoenvironmental reconstruction from chemical and isotopic compositions of Permo-Pennsylvanian pedogenic minerals, *Geochimica et Cosmochimica Acta*, *66*(17), 3093-3107. https://doi.org/10.1016/S0016-7037(02)00879-7.

Thomas, J., B. Parkash, and R. Mohindra (2002), Lithofacies and palaeosol analysis of the Middle and Upper Siwalik Groups (Plio–Pleistocene), Haripur-Kolar section, Himachal Pradesh, India, *Sedimentary Geology*, *150*(3), 343-366. https://doi.org/10.1016/S0037-0738(01)00203-2.

Vennemann, T. W., A. Morlock, W. von Engelhardt, and T. K. Kyser (2001), Stable isotope composition of impact glasses from the Nördlinger Ries impact crater, Germany, *Geochimica et Cosmochimica Acta*, *65*(8), 1325–1336. https://doi.org/10.1016/S0016-7037(00)00600-1.

Vennemann, T.W., O'Neil, J.R. (1993) A simple and inexpensive method of hydrogen isotope and water analyses of minerals and rocks based on zinc reagent. *Chemical Geology* 103, 227–234. https://doi.org/10.1016/0009-2541(93)90303-Z.

Verma, S., A. Mukherjee, R. Choudhury, and C. Mahanta (2015), Brahmaputra river basin groundwater: Solute distribution, chemical evolution and arsenic occurrences in different geomorphic settings, *Journal of Hydrology: Regional Studies*, *4*, 131–153. https://doi.org/10.1016/j.ejrh.2015.03.001.

Vitali, F., F. J. Longstaffe, P. J. McCarthy, A. G. Plint, and W. G. E. Caldwell (2002), Stable isotopic investigation of clay minerals and pedogenesis in an interfluve paleosol from the Cenomanian Dunvegan Formation, NE British Columbia, Canada, *Chemical Geology*, *192*(3), 269-287. https://doi.org/10.1016/S0009-2541(02)00225-5.

Vögeli, N., Huyghe, P., van der Beek, P., Najman, Y., Garzanti, E. and Chauvel, C., 2017. Weathering regime in the Eastern Himalaya since the mid-Miocene: Indications from detrital geochemistry and clay mineralogy of the Kameng River Section, Arunachal Pradesh, India. *Basin Research*. 30: 59–74. doi: 10.1111/bre.12242.

Von Blanckenburg, F. (2005), The control mechanisms of erosion and weathering at basin scale from cosmogenic nuclides in river sediment, *Earth and Planetary Science Letters*, *237*(3), 462-479. https://doi.org/10.1016/j.epsl.2005.11.017.

Whipple, K. X. (2009), The influence of climate on the tectonic evolution of mountain belts, *Nature Geoscience*, *2*(2), 97-104. doi:10.1038/ngeo413.

Willenbring, J. K., and F. von Blanckenburg (2010), Long-term stability of global erosion rates and weathering during late-Cenozoic cooling, *Nature*, *465*(7295), 211-214. doi:10.1038/nature09044.

Yeh, H.W. 1980) DH ratios and late-stage dehydration of shales during burial. *Geochimica et Cosmochimica Acta*, *44*(2), 341-352. https://doi.org/10.1016/0016-7037(80)90142-8.

Zachos, J. C., N. J. Shackleton, J. S. Revenaugh, H. Palike, and B. P. Flower (2001), Climate response to orbital forcing across the Oligocene-Miocene boundary, *Science*, *292*(5515), 274-278. DOI: 10.1126/science.1058288.